Sound & Vibration 2026, 60(1), 3752.
doi: https://doi.org/10.59400/sv3752

Article

Damping ratio measurements of multi-degree-of-freedom systems

Md. Mahbub Alam[1,*], Feiran Chen[1], Hongjun Zhu[2], Chunning Ji[3], Mostafa Zeinoddini[4], Vahid Tamimi[5], Tinghai Cheng[6]

[1] Center for Turbulence Control, Harbin Institute of Technology (Shenzhen), Shenzhen 518055, China
[2] State Key Laboratory of Oil and Gas Reservoir Geology and Exploitation, Southwest Petroleum University, Chengdu 610500, China
[3] State Key Laboratory of Hydraulic Engineering Intelligent Construction and Operation, Tianjin University, Tianjin 300350, China
[4] Faculty of Civil Engineering, K.N. Toosi University of Technology, Tehran 19697-64499, Iran
[5] School of Civil Engineering, Iran University of Science and Technology, Tehran 16846-13114, Iran
[6] Beijing Institute of Nanoenergy and Nanosystems, Chinese Academy of Sciences, Beijing 101400, China
*** Corresponding author:** Md. Mahbub Alam, alamm28@yahoo.com or alam@hit.edu.cn

CITATION

Alam MM, Chen F, Zhu H, et al. Damping ratio measurements of multi-degree-of-freedom systems. Sound & Vibration. 2026; 60(1): 3752. https://doi.org/10.59400/sv3752

ARTICLE INFO

Received: 5 November 2025
Revised: 27 January 2026
Accepted: 2 February 2026
Available online: 5 February 2026

Abstract: Accurate estimation of modal damping ratios is essential for predicting and controlling the dynamic response of multi-degree-of-freedom (MDOF) structures, particularly in bridge and structural vibration studies. Despite the availability of various methods for estimating damping ratios in MDOF systems, most approaches rely on modal decoupling, which often involves considerable complexity and effort. This work introduces two approaches that eliminate the need for modal decoupling: a filter-based method and an improved Half-Quadratic Gain Method (HQGM). The filter-based approach extracts decay characteristics directly from displacement signals using frequency-domain filtering and logarithmic envelope analysis, achieving damping ratio estimates within 3% error for both free and forced vibrations and for systems with low or high damping. The HQGM, originally formulated for single-degree-of-freedom systems, is extended here to MDOF systems and further enhanced by a correction formula that suppresses coupling-induced secondary peaks in frequency response functions. Comparative analysis demonstrates that while the original HQGM performs well in weakly coupled systems, the improved HQGM yields superior accuracy under strong coupling conditions. Both methods provide a robust framework for identifying damping characteristics across a wide range of dynamic systems. The proposed techniques offer practical advantages for structural engineering applications, where damping properties are difficult to measure directly.

Keywords: modal damping ratio; MDOF systems; filter-based method; HQGM; modal coupling

1. Introduction

Bridge vibration incidents resulting from wind-structure interaction have underscored the critical importance of accurate damping identification in structural engineering and design. In particular, the ability of a bridge to dissipate dynamic energy plays a key role in ensuring structural safety and serviceability under wind-induced excitations. As long-span bridges continue to increase in size, flexibility, and complexity, their dynamic behavior becomes more difficult to predict and control. This evolution has made the precise estimation of damping ratios in multi-degree-of-freedom (MDOF) systems not only more challenging but also more essential. Reliable damping measurements are fundamental to the development of

realistic analytical models, effective vibration mitigation strategies, and robust design practices that account for aeroelastic effects and resonance phenomena in large-scale bridge structures.

Environmental factors, such as traffic loads and wind effects, significantly influence the dynamic response of structures, including both urban transportation infrastructure and wind turbine blades [1]. These factors introduce time-varying forces and fluctuations that can alter the structural damping characteristics [2]. Traffic loads, for example, generate dynamic forces that vary depending on vehicle speed, weight, and traffic density. As seen in the Humen Bridge, the damping ratio increases from 0.069% under unloaded conditions to 0.290% when subjected to traffic-induced excitation [3]. Similarly, wind effects, including changes in wind pressure and turbulence, contribute additional dynamic loading, further affecting the structural damping and overall performance.

The single-degree-of-freedom (SDOF) system forms the fundamental basis for vibration analysis and provides essential insights into the modal decomposition of MDOF systems [4,5]. In a NASA technical memorandum, six commonly used methods for estimating the damping ratio of SDOF systems are summarized: the Half-Power Method, the HQGM, the Logarithmic Decrement Method, the Autocorrelation and Power Spectral Density Method, the Frequency Response Function (FRF) Method, and the Random Decrement Method [6]. Building upon these SDOF-based techniques, researchers have developed a variety of approaches to estimate damping ratios in MDOF systems, aiming to address the added complexity introduced by mode coupling and closely spaced natural frequencies.

Naylor et al. [7] introduced the Resonant Decay Method (RDM) for identifying the modal mass, damping, and stiffness matrices of MDOF systems exhibiting non-proportional damping. The effectiveness of the RDM was demonstrated using an analog plate model equipped with discrete dampers. The study further examined the influence of factors such as out-of-bandwidth flexible and rigid modes, imperfect force distribution, measurement noise, and deviations in mode shapes. While the RDM proved effective for systems with non-proportional damping, its performance degraded in the presence of non-smooth signals. To address this limitation, the researchers incorporated wavelet transform techniques, enabling improved handling of non-smooth and transient data. Meo et al. [8] proposed a wavelet transform–based method for estimating modal parameters of suspension bridges from time-domain output data. The Random Decrement Technique (RDT) was used to extract free vibration signals, which were then decomposed using wavelet transforms to identify natural frequencies, mode shapes, and damping ratios. This approach enhanced the analysis of non-stationary signals and, with the use of analytic wavelet transforms, offered improved time–frequency resolution for systems with closely spaced or dense modes.

Wang and Zhai [9] proposed a method for identifying modal damping ratios in MDOF systems with dense modes using the analytic wavelet transform. They constructed normalized analytic wavelets to transform system responses into wavelet magnitude maps, from which ridge points were extracted. The damping ratio of each

mode was then estimated from the corresponding logarithmic magnitude curves. To improve the accuracy and robustness of data analysis, Ku et al. [10] proposed a Random Decrement (RD) method that integrates Fast Fourier Transform (FFT) and Linear Least Squares. This approach enables accurate modal identification even without knowledge of external excitation, making it effective in complex and variable environments.

To address nonlinear and nonsmooth vibration signals, He et al. [11] proposed a method combining Empirical Mode Decomposition (EMD) with the RD. The Newton–Raphson iterative method, coupled with the Davidon–Fletcher–Powell (DFP) variable scaling algorithm, was used to obtain optimal solutions. This approach improves parameter identification accuracy while reducing errors caused by signal irregularities. In bridge modal analysis, distinguishing between free and forced vibration remains a key challenge. To address this, Yang et al. [12] proposed the Iterative Variational Modal Decomposition (IVMD) method, which automatically extracts individual modal components from free vibration data without manual intervention. The identified free vibration signals are then processed using the data-dependent Eigensystem Realization Algorithm (ERA) to estimate modal parameters.

The impact of environmental loads, such as traffic and wind, on the modal damping of suspension bridges has become an important research focus. Dan et al. [13] studied how traffic and wind loads affect the dynamic characteristics of suspension bridges. Using the Extended Dynamic Stiffness Method (EDSM), they derived an explicit expression for the modal damping ratio under traffic loading and established its relationship with bridge design parameters. Their findings show that modal damping increases with traffic load, which helps suppress wind-induced vortex-excited vibrations. Niu et al. [14] proposed a method for identifying modal parameters of multi-span bridges by combining Complementary Ensemble Empirical Mode Decomposition (CEEMD) with the RDT. Utilizing high-frequency GNSS-RTK measurements to capture dynamic responses, this approach improves the accuracy and reliability of modal identification under operational conditions.

Advancements in vibration signal analysis have led to non-contact methods that simplify testing and improve measurement accuracy. Hallal et al. [15] introduced a video amplification technique to identify modal damping ratios in mechanical structures. Using a high-frame-rate camera, they captured the vibration response of a cantilever beam subjected to shock. The structure's FRF was extracted via video amplification, and damping ratios were calculated using the 3 dB bandwidth method.

The HQGM was originally developed for SDOF systems as a robust technique for estimating damping ratios from FRFs using the half-power points [16, 17]. The method has been widely utilized due to its ability to provide accurate damping estimates in systems with low to moderate damping. The HQGM has been further explored and applied in various domains, including mechanical systems and vibration analysis [18,19]. However, its direct application to multi-degree-of-freedom (MDOF) systems, where modal coupling and closely spaced modes often occur, presents significant challenges. In MDOF systems, coupling effects can distort the FRF, leading to inaccurate damping estimates. Recent studies have attempted to extend the HQGM to MDOF systems

by incorporating modal decoupling techniques or alternative methods to address these issues [8]. Despite these efforts, the accuracy of the HQGM remains compromised in systems with strong coupling.

Although many methods exist for estimating damping ratios in MDOF systems, most require modal decoupling, leading to significant effort. We propose two novel methods for estimating damping ratios in 2DOF systems: a filter-based method that avoids modal decoupling and an improved HQGM that corrects coupling-induced errors, offering more efficient and accurate results compared to existing techniques. The first is a filter-based approach that extracts decay characteristics directly from displacement signals to estimate damping ratios. The second is an enhanced version of the HQGM—originally developed for SDOF systems and detailed in NASA's technical manual—augmented with a correction formula to extend its application to MDOF systems. This study extends beyond existing methods such as wavelet transforms and RDT, not merely complementing but offering a distinct and more efficient framework for damping estimation. By addressing the challenges of modal decoupling and computational effort, the present methods provide a more accessible and accurate solution for structural applications.

The remainder of this paper is organized as follows. The filter-based damping estimation method and its application to both excited and unexcited 2DOF systems are presented in Section 2. The original HQGM and its improved version for handling modal coupling are introduced in Section 3, along with validation under different coupling conditions. Summary of key findings and concluding remarks are provided in Section 4.

2. Filter-based method for damping estimation

2.1. Application to unexcited 2DOF systems

The dynamic equation of a 2DOF unexcited system, in the absence of excitation, is given by Liu et al. [20]:

$$[M]\{\ddot{X}\} + [C]\{\dot{X}\} + [X]\{X\} = 0 \tag{1}$$

where M denotes the mass matrix, C is the damping matrix, and K is the stiffness matrix. The vectors X, $\dot{X}$, and $\ddot{X}$ denote displacement, velocity, and acceleration of the system, respectively.

A simple sketch of an unexcited 2DOF is shown in **Figure 1a**, where subscripts '1' and '2' refer to the structures '1' and '2', respectively. The specific equations of motion for this system can be derived as

$$\begin{aligned} m_1\ddot{x}_1 + c_1\dot{x}_1 + (k_1 + k_2)\, x_1 - k_2 x_2 = 0 \\ m_2\ddot{x}_2 + c_2\dot{x}_2 - k_2 x_1 + k_2 x_2 = 0 \end{aligned} \tag{2}$$

The final expressions for the displacements of the system are as follows:

$$\begin{aligned} x_1(t) = A_{11}e^{\alpha_1 t}\cos(\beta_1 t) + A_{12}e^{\alpha_2 t}\cos(\beta_2 t) \\ x_2(t) = A_{21}e^{\alpha_1 t}\cos(\beta_1 t) + A_{22}e^{\alpha_2 t}\cos(\beta_2 t) \end{aligned} \tag{3}$$

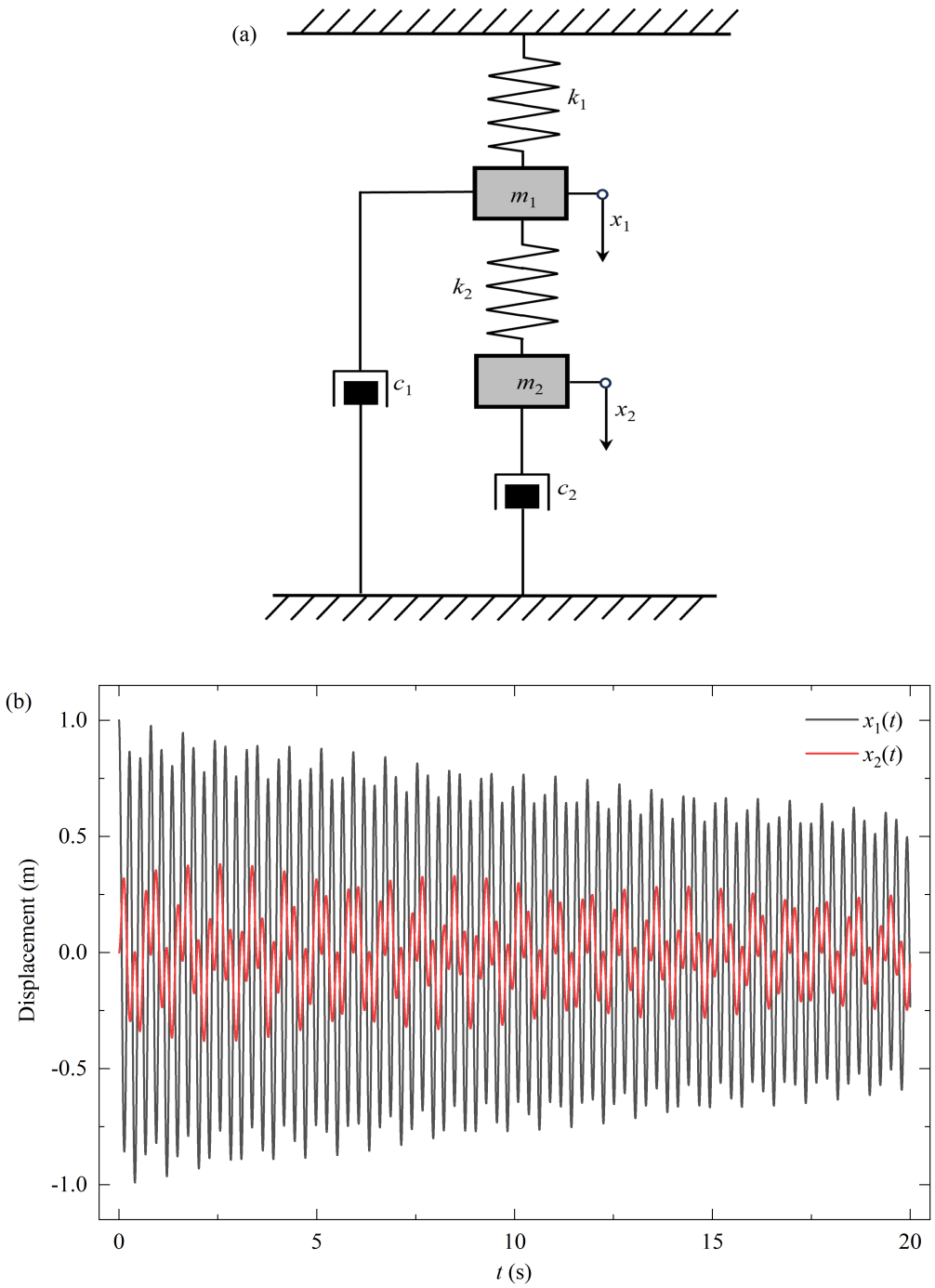

Figure 1. **(a)** Free vibration of a 2DOF system; **(b)** Vibration displacement response of a 2DOF unexcited system.

Our goal is to deepen the understanding of the fundamental vibration responses of a forced damped system. In this context, we introduce universal definitions for the frequency ratio and critical damping ratio, which are essential for effectively teaching and learning the mechanics of a damped system subjected to an excitation force. There is no doubt that this content is imperative and indispensable for pupils, teachers, researchers, engineers, and military personnel. The constants A_{11}, A_{12}, A_{21}, and A_{22} are the inherent characteristics of the system, determined by the initial conditions. The parameters α_1 or α_2 and β_1 or β_2 represent the corresponding mode decay factor and damped natural frequency, respectively, both of which depend solely on the intrinsic

properties of the system.

It can be seen that both displacement expressions are linear combinations of $e^{\alpha_1 t}cos\,(\beta_1 t)$ and $e^{\alpha_2 t}cos\,(\beta_2 t)$. To analyze the system and produce response signals, the following parameter values are selected: m_1 = 1 kg, m_2 = 2 kg, c_1 = 0.05 Nm/s, c_2 = 0.1 Nm/s, k_1 = 300 N/m, k_2 = 200 N/m. The initial conditions are set as: $x_1(0)$ = 1 m, $\dot{x}_1(0)$ = 0 m/s, $x_2(0)$ = 0 m, and $\dot{x}_2(0)$ = 0 m/s. Using these values, the displacement response of the system can be explicitly calculated as:

$$\begin{aligned} x_1(t) &= 0.9092e^{-0.025t}cos(23.344t) - 0.00097e^{-0.025t}sin(23.344t) \\ &\quad +0.0918e^{-0.025t}cos(7.420t) - 0.00031e^{-0.025t}sin(7.420t) \\ x_2(t) &= -0.2044e^{-0.025t}cos(23.344t) + 0.00022e^{-0.025t}sin(23.344t) \\ &\quad +0.2040e^{-0.025t}cos(7.420t) - 0.00069e^{-0.025t}sin(7.420t) \end{aligned} \tag{4a}$$

Neglecting very small-amplitude terms, Equation (4a) could be reduced to

$$\begin{aligned} x_1(t) &= 0.9092e^{-0.025t}cos(23.344t) + 0.0918e^{-0.025t}cos(7.420t) \\ x_2(t) &= -0.2044e^{-0.025t}cos(23.344t) + 0.2040e^{-0.025t}cos(7.420t) \end{aligned} \tag{4b}$$

The corresponding displacement responses of the system are illustrated in **Figure 1b**.

For a 2DOF system, the system matrix is a 4 × 4 real matrix, and its eigenvalues typically appear as two pairs of complex conjugates, expressed as $\lambda = -\alpha \pm j\beta$, where α represents the decay factor, and β is the damped natural frequency for the corresponding mode. According to the theory of linear differential equations with constant coefficients, each pair of complex conjugate eigenvalues corresponds to a modal solution of the form $e^{-\alpha t}cos(\beta t)$ and $e^{-\alpha t}sin(\beta t)$. The general solution of the system's displacement response is then a linear combination of such modal components, each representing one mode of vibration. When the initial conditions are applied, the specific coefficients of each mode are determined, and the final expression for the displacement response becomes an explicit sum of exponentially decaying sinusoidal terms.

As a result, each term in the response expression clearly contains an exponential decay component $e^{-\alpha t}$, representing the damping factor α, and a cosine wave $cos(\beta t)$ or sin wave $sin(\beta t)$ with the damped natural frequency β. Since this structure arises directly from the eigenvalue characteristics of the system, the parameters α and β can be extracted from the response expression with mathematical rigor.

For a single degree of freedom of a system, the displacement equation can be written as,

$$x(t) = Ae^{-\zeta\omega_n t}cos\left(\omega_n\sqrt{1-\zeta^2}t\right) \tag{5}$$

where A is a constant (depending on the initial condition), ζ is the damping ratio, and ω_n is the undamped natural frequency of the system. Here, the decay factor α and the

damped natural frequency can be expressed as,

$$\alpha = \zeta\omega_n \tag{6a}$$

$$\beta = \omega_n\sqrt{1-\zeta^2} \tag{6b}$$

Equation (5) can now be written as,

$$x(t) = Ae^{-\alpha t}cos(\beta t) \tag{7}$$

The ζ can be obtained by solving Equation (6a,b) as,

$$\zeta = \frac{\alpha}{\sqrt{\alpha^2+\beta^2}} \tag{8}$$

Equation (8) has been used to calculate the damping ratio in the study of Casiano [6]. From Equation (4), the first mode of the system has a decay factor of 0.025 and a damped natural frequency of 7.420 rad/s, yielding a damping ratio of 0.00337. The second mode, with the same decay factor of 0.025 and a natural frequency of 23.344 rad/s, corresponds to a damping ratio of 0.00107. These values represent the actual modal damping ratios of the unexcited system.

Given the relationship between circular frequency and frequency,

$$f_n = \frac{\omega_n}{2\pi} \tag{9}$$

the corresponding frequencies are calculated as f_{n1} = 1.18 Hz and f_{n2} = 3.72 Hz.

In practical and engineering applications, the mass, damping, and stiffness of a system are often difficult to determine directly, whereas vibration displacement responses can be readily measured using sensors and other tools. In the following sections, we present a method for extracting the system's natural frequencies and damping ratios based on the measured displacement response.

The FFT is a powerful tool for analyzing the frequency content of a signal. It converts complex time-domain signals into the frequency domain, revealing the underlying frequency characteristics. Here, two vibration displacement responses x_1 and x_2 are analyzed using FFT to identify the dominant vibration frequencies of the system. The resulting FFT power spectra are shown in **Figure 2**.

To facilitate comparison of spectral characteristics across different frequency ranges and eliminate the influence of absolute amplitude scales, the FFT amplitude spectra were normalized by dividing all values by the maximum amplitude within the analyzed frequency range. This normalization approach allows for dimensionless representation of the frequency content, making it easier to identify dominant frequency components and compare relative amplitude distributions. As shown in **Figure 2**, the two vibration displacement signals (from **Figure 1b**) exhibit two dominant vibration frequencies each. The two frequency values (f_1 = 1.17 Hz and f_2 = 3.70 Hz) are identical for both signals, while their amplitudes differ, as expected. These frequency values closely match those calculated from Equation (6), with minor errors of 1.22% and 0.41%, respectively, attributed to the FFT frequency resolution. Thus, the natural

frequencies derived from the FFT method can be considered accurate.

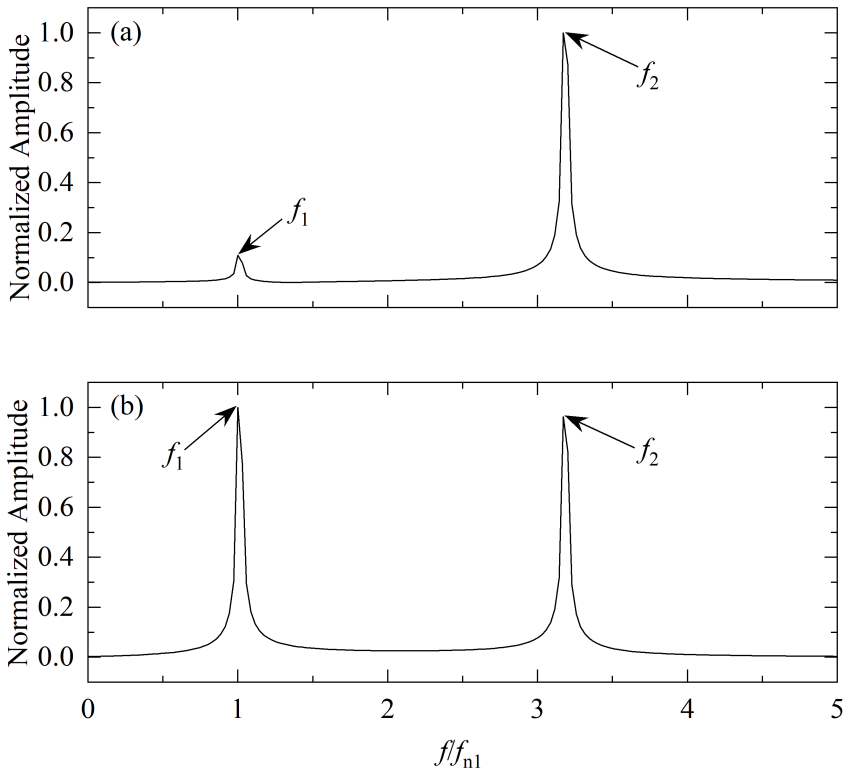

Figure 2. Amplitude-frequency curves obtained by FFT of vibration displacement responses of a 2DOF unexcited system: FFT of **(a)** $x_1(t)$; **(b)** $x_2(t)$.

Using f_1 and f_2 as the center frequencies, corresponding bandpass filters are designed to isolate the displacement responses in **Figure 1b**. The filter bandwidth is set to 20% of the center frequency, with the lower and upper cutoff frequencies defined as 0.9 and 1.1 times the center frequency, respectively, following Köhler et al. [21]. This filtering process allows the system's responses associated with each frequency to be separated and analyzed individually. As an example, the displacement response x_1 is filtered, and the resulting signal is shown in **Figure 3**. Both filtered signals exhibit amplitude decay over time. Since the damping ratio is determined using the decay factor α and the oscillation frequency β (as shown in Equation (8)), a key question arises: can α be reliably estimated from the filtered signals for accurate damping ratio calculation? How is α extracted from a signal? Is it represented by the slope of the envelope connecting the signal peaks? If so, is this envelope always linear? If the decay is not linear, what method should be used to calculate α? Note that the circular frequency β has already been determined from the FFT results in **Figure 2**.

Recalling the equation $x(t) = Ae^{-\alpha t}cos(\beta t)$, the amplitude envelope is,

$$A_p(t) = Ae^{-\alpha t}. \tag{10}$$

Taking the logarithm on both sides of the equation, we can get:

$$ln(A_p(t)) = lnA - \alpha t. \tag{11}$$

It is now a straight line equation, with a negative slope of α magnitude that is to

be calculated from the signal as shown in **Figure 4**.

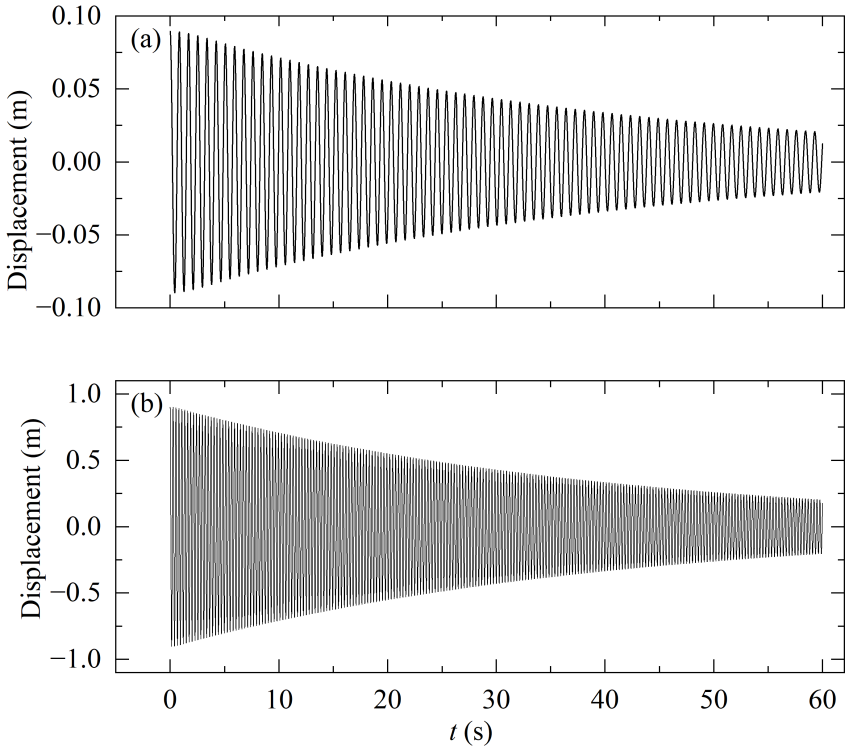

Figure 3. Filtered modal components of displacement $x_1(t)$ for the 2DOF system: First and second modal components centered at **(a)** f_1 = 1.17 Hz; **(b)** f_2 = 3.70 Hz, respectively.

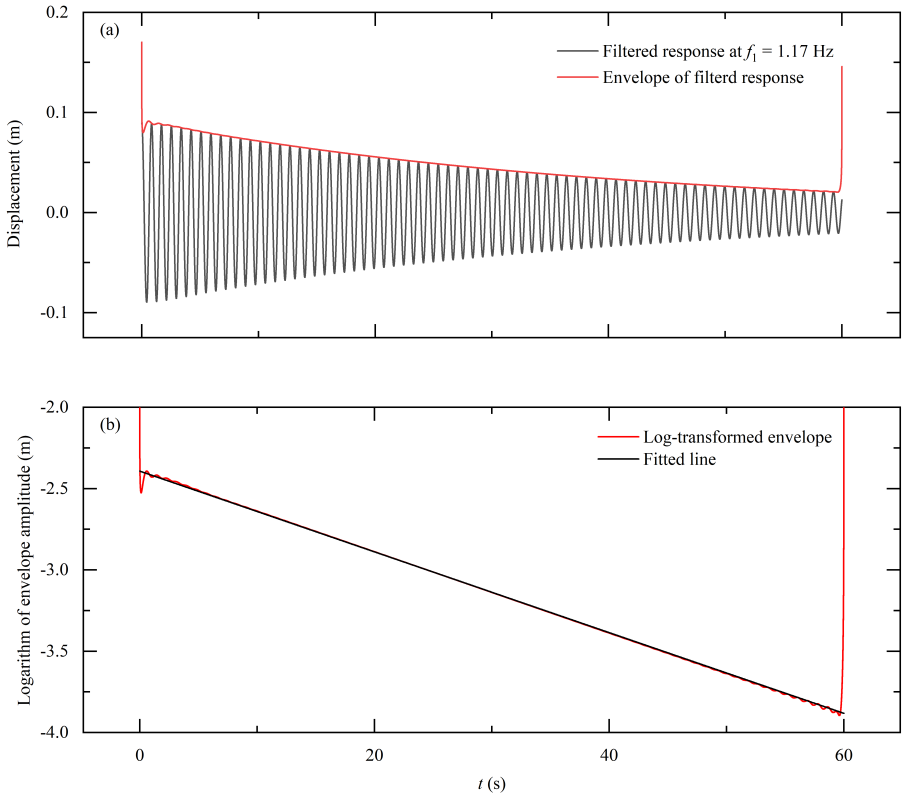

Figure 4. **(a)** First mode component of displacement $x_1(t)$ and its envelope, centered at f_1 = 1.17 Hz; **(b)** Log-transformed envelope of the first mode and its linear fit.

Firstly, the Hilbert transform is used on the filtered signals to get the envelope of

the curve, as shown in **Figure 4a**. The estimated α and β of the system given in this example are shown in **Table 1**.

Table 1. Decay factor and natural frequency of the unexcited system.

	Estimated α_1 ($\times 10^{-2}$)	Estimated β_1	Estimated α_2 ($\times 10^{-2}$)	Estimated β_2
$x_1(t)$	2.447	7.420	2.495	23.344
$x_2(t)$	2.441	7.420	2.492	23.344

After obtaining β and α of the system, ζ values for the two modes can be calculated directly using Equation (8). The actual modal damping ratios $\zeta_1 = 3.369 \times 10^{-3}$ and $\zeta_2 = 1.071 \times 10^{-3}$ are obtained from Equation (4). The results of the calculations and the error are shown in **Table 2**.

Table 2. Damping ratios and errors by filter-based method (unexcited system).

Mode	Input	Frequencies (Hz)	Estimated ζ ($\times 10^{-3}$)	Actual ζ ($\times 10^{-3}$)	Errors in ζ
ζ_1	$x_1(t)$	1.17	3.298	3.369	2.12%
	$x_2(t)$	1.17	3.290	3.369	2.36%
ζ_2	$x_1(t)$	3.70	1.069	1.071	0.20%
	$x_2(t)$	3.70	1.068	1.071	0.32%

As shown in **Table 2**, the errors are all below 2.36%. This demonstrates that the filter-based method can accurately estimate the damping ratios of an unexcited 2DOF system.

After isolating the vibration response of a single mode through filtering, the logarithmic decrement method — commonly used for SDOF systems [22–25]—can also be employed to estimate the system's damping ratio. The results obtained by applying the traditional logarithmic decrement method to the system presented in this section are provided in **Table 3**.

Table 3. Damping ratios and errors by logarithmic decrement method (unexcited system).

Mode	Input	Frequencies (Hz)	Estimated ζ ($\times 10^{-3}$)	Actual ζ ($\times 10^{-3}$)	Errors in ζ
ζ_1	$x_1(t)$	1.17	3.3191	3.3693	1.49%
	$x_2(t)$	1.17	3.3218	3.3693	1.41%
ζ_2	$x_1(t)$	3.70	1.0669	1.0709	0.38%
	$x_2(t)$	3.70	1.0712	1.0709	0.02%

The logarithmic decrement method is highly dependent on the quality of the filtered signal. If the filtered signal accurately reflects the true decay behavior, the resulting damping ratio estimation can be precise. By comparing the calculation errors presented in **Tables 2** and **3**, it can be seen that the filtered signals used in this study are of high quality. Under such conditions, the logarithmic decrement method yields even more accurate results.

2.2. Application to 2DOF excited systems

The dynamic equation of a 2DOF system under excitation is given by

$$[M]\{\ddot{X}\} + [C]\{\dot{X}\} + [K]\{X\} = F(t), \tag{12}$$

where $F(t)$ denotes the excitation force. The corresponding 2DOF schematic is provided in **Figure 5a**.

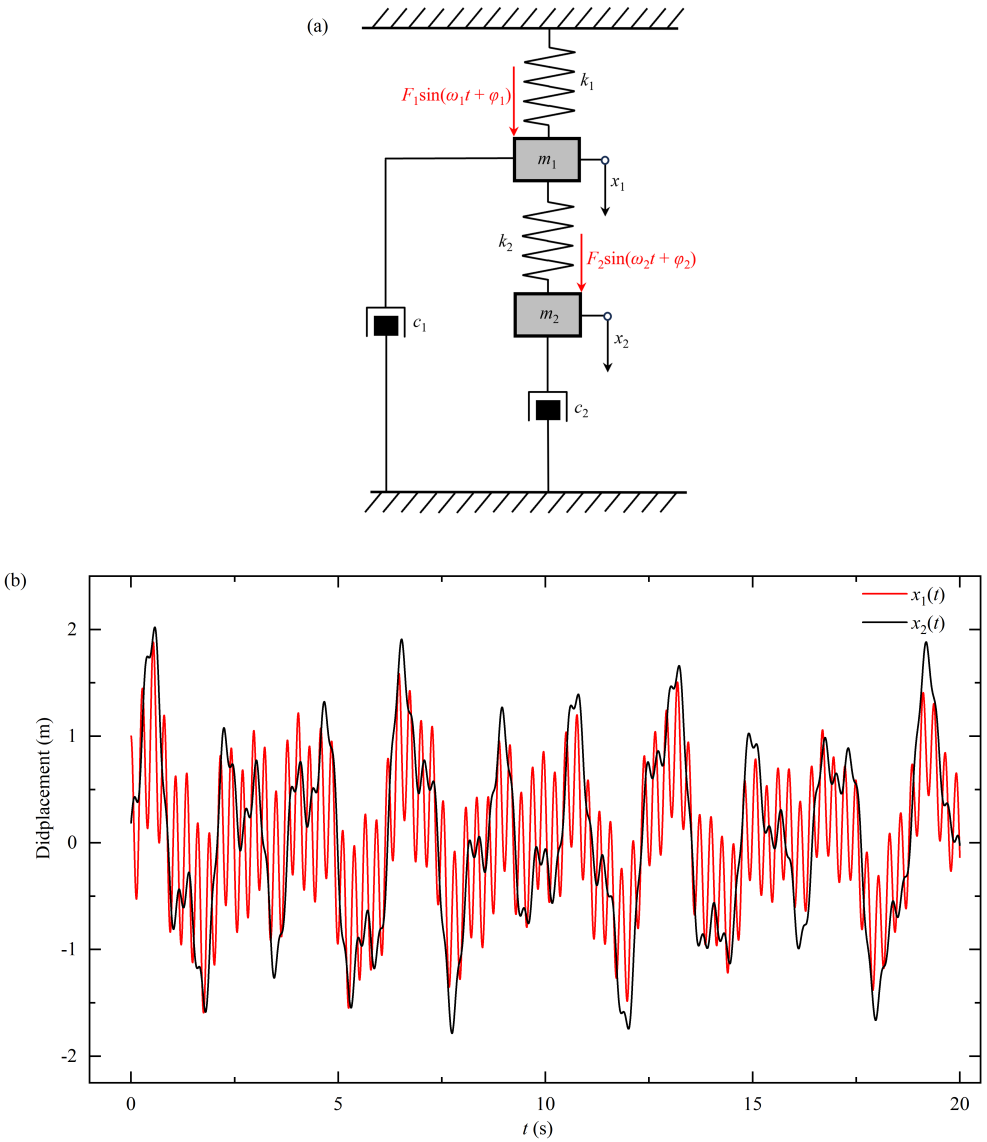

Figure 5. **(a)** Forced vibration of a 2DOF system; **(b)** Vibration displacement response of a 2DOF excited system.

The equation of motion for an unexcited system is a homogeneous system of equations. In contrast, when the system is subjected to external excitation, the equation of motion becomes nonhomogeneous, with the additional terms accounting for the applied external forces. The nonhomogeneous system is shown as follows.

$$\begin{aligned} m_1\ddot{x}_1 + c_1\dot{x}_1 + (k_1+k_2)\,x_1 - k_2x_2 &= F_1 sin\,(\omega_1 t+\phi_1) \\ m_2\ddot{x}_2 + c_2\dot{x}_2 - k_2x_1 + k_2x_2 &= F_2 sin\,(\omega_2 t+\phi_2) \end{aligned} \tag{13}$$

where F_1 and F_2 denote the amplitude of external forces, ω_1 and ω_2 denote the circular frequency of external forces, and ϕ_1 and ϕ_2 denote the corresponding phase lag with respect to the initial conditions. The above six known physical quantities are all constants: F_1 = 120 N, F_2 = 100 N, ω_1 = 2 rad/s, ω_2 = 3 rad/s, ϕ_1 = 0.5 rad, and ϕ_2 = 0.4 rad. The specific values of physical quantities such as mass, damping, and

stiffness are the same as those in the unexcited system described in Section 2.1.

The solution to a nonhomogeneous system of equations consists of two: the complementary solution to the corresponding homogeneous system and a particular solution to the nonhomogeneous system. The first step is to determine the particular solution.

Decomposing the external force using the trigonometric sum and difference formulas, we can get:

$$\begin{aligned} F_1 sin\left(\omega_1 t+\phi_1\right) &= F_1\left[sin\left(\omega_1 t\right) cos\phi_1 + cos\left(\omega_1 t\right) sin\phi_1\right] \\ F_2 sin\left(\omega_2 t+\phi_2\right) &= F_2\left[sin\left(\omega_2 t\right) cos\phi_2 + cos\left(\omega_2 t\right) sin\phi_2\right] \end{aligned} \tag{14}$$

In this system, the external excitation comprises multiple frequency components, and the system must respond to each accordingly. The response at each degree of freedom is influenced by all frequency components, with the response to each frequency consisting of both sine and cosine terms. Consequently, four unknown coefficients must be determined for each degree of freedom to fully describe the amplitude and phase of the sine and cosine components associated with each frequency. Given that the system has two degrees of freedom and is subjected to two distinct frequency components, the particular solution involves a total of eight unknown coefficients. The particular solutions can then be expressed as follows.

$$\begin{aligned} x_{1,p}(t) &= A_1 sin\left(\omega_1 t\right) + B_1 cos\left(\omega_1 t\right) + C_1 sin\left(\omega_2 t\right) + D_1 cos\left(\omega_2 t\right) \\ x_{2,p}(t) &= A_2 sin\left(\omega_1 t\right) + B_2 cos\left(\omega_1 t\right) + C_2 sin\left(\omega_2 t\right) + D_2 cos\left(\omega_2 t\right) \end{aligned} \tag{15}$$

After defining the particular solution with eight unknown coefficients, take its first and second derivatives, substitute them into Equation (13), and match the coefficients of sin and cos. This yields eight linear equations that naturally split into two independent 4×4 subsystems: the first contains the unknowns A_1, B_1, A_2, B_2 together with F_1 and ω_1; the second contains the unknowns C_1, D_1, C_2, D_2 together with F_2 and ω_2. Solving each 4×4 system individually provides its corresponding coefficients. These two 4×4 systems of equations are given as follows.

$$\begin{pmatrix} k_1+k_2-m_1\omega_1^2 & -k_2 & \omega_1 c_1 & 0 \\ -k_2 & k_2-m_2\omega_1^2 & 0 & \omega_1 c_2 \\ -\omega_1 c_1 & 0 & k_1+k_2-m_1\omega_1^2 & -k_2 \\ 0 & -\omega_1 c_2 & -k_2 & k_2-m_2\omega_1^2 \end{pmatrix} \begin{pmatrix} A_1 \\ A_2 \\ B_1 \\ B_2 \end{pmatrix} = \begin{pmatrix} F_1 cos\phi_1 \\ 0 \\ F_1 sin\phi_1 \\ 0 \end{pmatrix} \tag{16}$$

$$\begin{pmatrix} k_1+k_2-m_1\omega_2^2 & -k_2 & \omega_2 c_1 & 0 \\ -k_2 & k_2-m_2\omega_2^2 & 0 & \omega_2 c_2 \\ -\omega_2 c_1 & 0 & k_1+k_2-m_1\omega_2^2 & -k_2 \\ 0 & -\omega_2 c_2 & -k_2 & k_2-m_2\omega_2^2 \end{pmatrix} \begin{pmatrix} C_1 \\ C_2 \\ D_1 \\ D_2 \end{pmatrix} = \begin{pmatrix} 0 \\ F_2 cos\phi_2 \\ 0 \\ F_2 sin\phi_2 \end{pmatrix} \tag{17}$$

After solving Equations (16) and (17), the eight unknown coefficients are obtained: A_1 = 0.3659, A_2 = 0.3809, B_1 = 0.2004, B_2 = 0.2091, C_1 = 0.3726, C_2 = 0.9149, D_1 = 0.1591, D_2 = 0.3903. After substituting the above data into Equation (15), the particular

solution of Equation (13) can be obtained as

$$\begin{aligned} x_{1,p}(t) &= 0.3659sin(2t) + 0.2004cos(2t) + 0.3726sin(3t) + 0.1591cos(3t) \\ x_{2,p}(t) &= 0.3809sin(2t) + 0.2091cos(2t) + 0.9149sin(3t) + 0.3903cos(3t) \end{aligned} \tag{18}$$

The homogeneous solution of the system is subsequently determined. In this study, the forced vibration system is subjected to the same initial conditions as the free vibration system analyzed in Section 2.1. Given that the particular solution of the forced system has already been derived, the initial conditions corresponding to the homogeneous solution at t = 0 s can be obtained accordingly. Utilizing these initial conditions, the homogeneous solution can be computed following the same procedure outlined in Section 2.1. By superimposing the homogeneous and particular solutions, the complete displacement response of the forced vibration system is thus obtained.

$$\begin{aligned} x_1(t) &= -0.1859e^{-0.025t}\cos(7.420t) - 0.2164e^{-0.025x}\sin(7.420t) \\ &\quad +0.8271e^{-0.025x}\cos(23.344t) - 0.0097e^{-0.025t}\sin(23.344t) + x_{1,p}(t) \\ x_2(t) &= -0.4138e^{-0.025t}\cos(7.420t) - 0.4815e^{-0.025t}\sin(7.420t) \\ &\quad +0.0022e^{-0.025t}\cos(23.344t) + 0.1858e^{-0.025t}\sin(23.344t) + x_{2,p}(t) \end{aligned} \tag{19}$$

The vibration displacement response of the system is shown in **Figure 5b**.

Since the undamped natural frequency is an inherent property of the system, the presence or absence of external forces does not affect it. Therefore, the natural frequency of the excited system should be equal to that of the unexcited system.

Using the FFT on the two vibration displacement signals separately, the vibration frequencies of the system can be known from **Figure 6**. As can be seen from **Figure 6**, the two vibration displacement curves have four predominant vibration frequencies: f_1 = 0.30 Hz, f_2 = 0.47 Hz, f_3 = 1.17 Hz, and f_4 = 3.70 Hz. Notably, f_1 and f_2 correspond exactly to the frequencies of the external forces, while f_3 and f_4 are the natural frequencies of the excited system. Moreover, these two frequencies are exactly equal to the natural frequencies of the unexcited system, as the damping values are small.

Using these four frequencies as center frequencies, corresponding filters are designed to process the vibration response signals in **Figure 5b**. This allows the displacement responses of the system to be isolated at each of these frequencies.

Filtering the response signals yields the results shown in **Figure 7**. It can be observed that the filtered signals at the excitation center frequencies f_1 and f_2 are not attenuated (**Figure 7a,b**). This indicates that the corresponding damping ratios are effectively zero; no evidence of structural damping is present at the excitation frequencies. In other words, damping at the excitation frequencies does not play a significant role. In contrast, the filtered signals at the system's natural frequencies f_3 and f_4 exhibit clear attenuation, revealing the influence of structural damping.

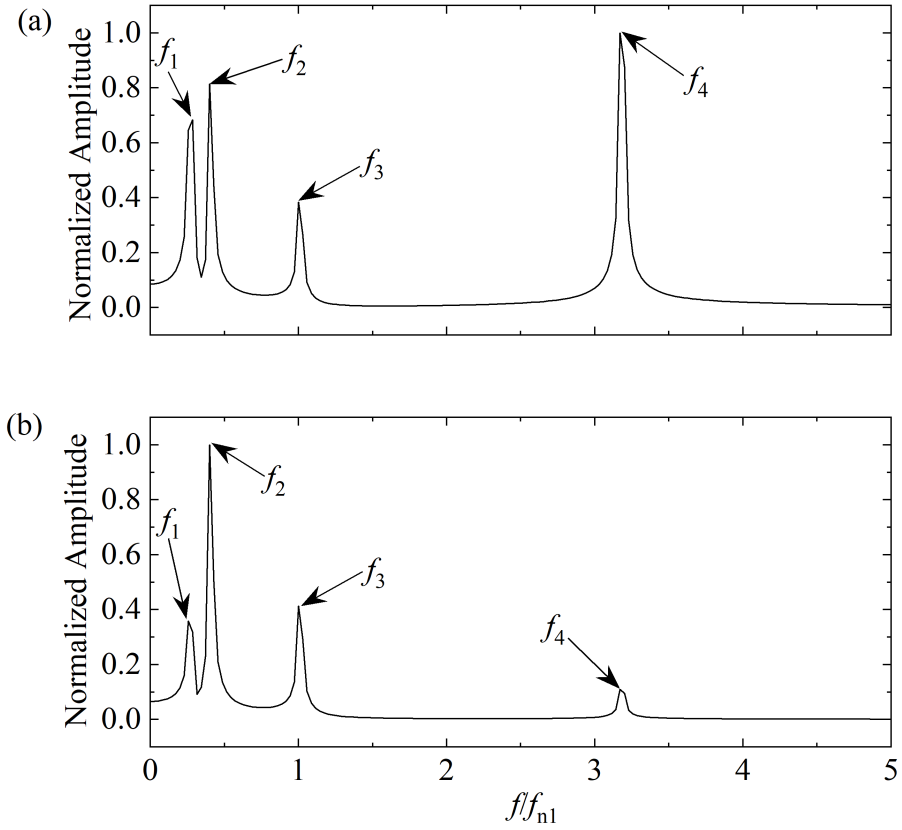

Figure 6. Amplitude-frequency curves obtained by FFT of vibration displacement responses of a 2DOF system with force: FFT of **(a)** $x_1(t)$; **(b)** $x_2(t)$.

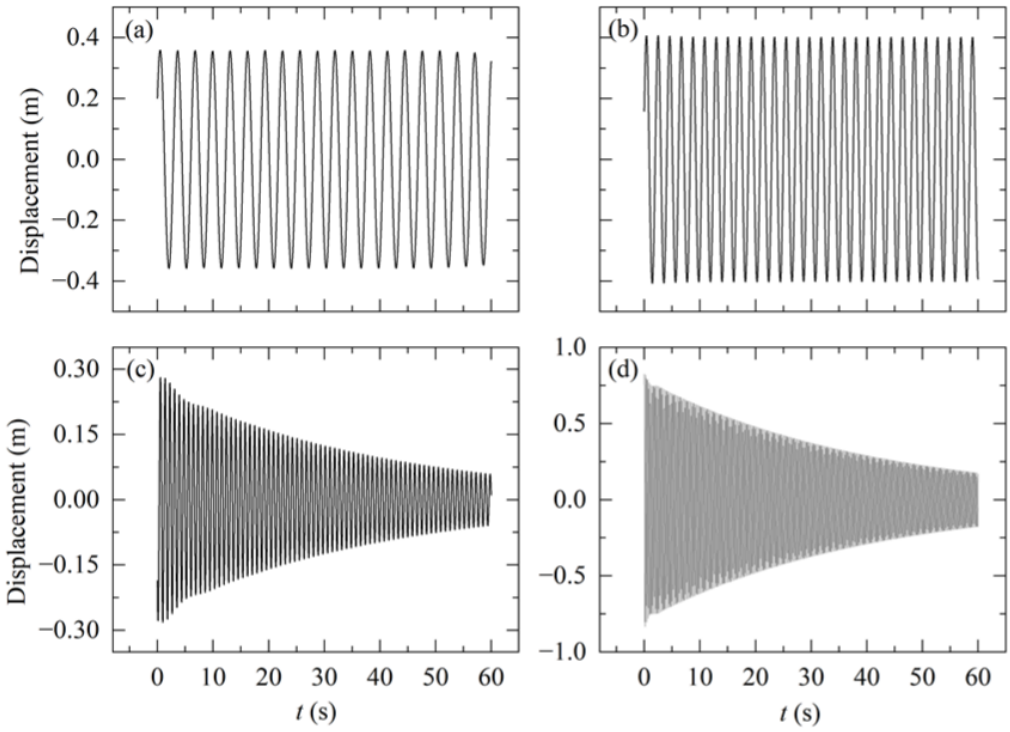

Figure 7. Filtered components of displacement response $x_1(t)$ centered at **(a)** f_1 = 0.3 Hz; **(b)** f_2 = 0.47 Hz; **(c)** f_3 = 1.17 Hz; **(d)** f_4 = 3.70 Hz.

Following the same procedure applied to the unforced system in Section 2.1, the decay factor α and the natural frequency β are estimated from the filtered signals, as

summarized in **Table 4**.

Table 4. Decay factor and natural frequency of the excited system.

	Estimated α_1 ($\times 10^{-2}$)	Estimated β_1	Estimated α_2 ($\times 10^{-2}$)	Estimated β_2
$x_1(t)$	2.519	7.420	2.533	23.344
$x_2(t)$	2.417	7.420	2.578	23.344

Using α and β values, the corresponding damping ratios are calculated and compared with the actual values in **Table 5**. The table shows that the deviation from the theoretical values is less than 3.12%, demonstrating both the feasibility and accuracy of the proposed method. The larger errors observed for (1.32% and 3.12%) compared to (0.76% and 0.68%) are primarily due to leakage from the first mode into the passband of the second mode. Although the frequency separation between the two modes is much greater than the filter's bandwidth, which usually ensures good mode separation, leakage remains an inherent limitation of the filter design. The six-order Butterworth filter used in this study, while effective, cannot fully eliminate this leakage. Notably, the errors indicate that the leakage is more pronounced at the higher frequency of 3.70 Hz. The selection of the 6th-order Butterworth filter was based on a balance between filter stability and sensitivity to bandwidth. The Butterworth filter is known for its maximally flat frequency response in the passband, which minimizes distortion and ensures reliable signal processing. It provides a good trade-off between filter sharpness and computational complexity. Higher-order filters can improve the attenuation of unwanted frequencies, but they can also lead to increased sensitivity and potential instability if not carefully tuned.

Table 5. Damping ratios and errors by filter-based method (excited system).

Mode	Input	Frequencies (Hz)	Estimated ζ ($\times 10^{-3}$)	Actual ζ ($\times 10^{-3}$)	Errors in ζ
ζ_1	$x_1(t)$	1.17	3.395	3.369	0.76%
	$x_2(t)$	1.17	3.392	3.369	0.68%
ζ_2	$x_1(t)$	3.70	1.085	1.071	1.32%
	$x_2(t)$	3.70	1.104	1.071	3.12%

For the same excited system, the damping ratio is calculated using the logarithmic decrement method and compared with that obtained from the envelope method. Comparison of **Tables 5** and **6** indicates that the logarithmic attenuation method and the filter-based method attain comparable computational accuracy. The former, nevertheless, exhibits a larger error variance, implying a pronounced dependence on signal quality. Accordingly, the filter-based method affords greater stability.

Table 6. Damping ratios and errors by logarithmic decrement method (excited system).

Mode	Input	Frequencies (Hz)	Estimated ζ ($\times 10^{-3}$)	Actual ζ ($\times 10^{-3}$)	Errors in ζ
ζ_1	$x_1(t)$	1.17	3.3444	3.3693	0.74%
	$x_2(t)$	1.17	3.2891	3.3693	2.38%
ζ_2	$x_1(t)$	3.70	1.0706	1.0709	0.03%
	$x_2(t)$	3.70	1.1055	1.0709	3.23%

As shown in **Tables 2** and **5**, when evaluating the accuracy of the filter-based method for calculating the damping ratios of a 2DOF system, the damping ratios of

the given system are very small, with the highest modal damping ratio not exceeding 0.005. Therefore, the filter-based method can be considered an effective and reliable technique for estimating the modal damping ratios in low-damping 2DOF systems.

2.3. Applications to systems with high damping ratio

To examine whether the filter-based method is applicable to systems with higher damping ratios, a new system is designed by adjusting parameters such as mass, stiffness, and damping. The newly adopted parameter values are: m_1 = 1 kg, m_2 = 1 kg, c_1 = 0.04 Nm/s, c_2 = 0.03 Nm/s, k_1 = 1 N/m, k_2 = 1 N/m. The damping ratio of the new system is calculated using the same method described in Section 2.1, and the results are presented in **Table 7**.

Table 7. Damping ratios and errors (higher-damping-ratio unexcited system).

Mode	Input	Frequencies (Hz)	Estimated ζ_e ($\times 10^{-2}$)	Actual ζ_a ($\times 10^{-2}$)	Errors in ζ
ζ_1	$x_1(t)$	0.10	2.6840	2.6506	1.26%
	$x_2(t)$	0.10	2.6602	2.6506	0.36%
ζ_2	$x_1(t)$	0.26	1.1337	1.1507	1.47%
	$x_2(t)$	0.26	1.1446	1.1507	0.52%

Subsequently, the applicability of the filter-based method is examined for the excited system with a higher damping ratio. An external force identical to that described in Section 2.2 is applied to this system, and its damping ratio is then computed. The results of the calculation are presented in **Table 8**.

Table 8. Damping ratios and errors (higher-damping-ratio excited system).

Mode	Input	Frequencies (Hz)	Estimated ζ ($\times 10^{-2}$)	Actual ζ ($\times 10^{-2}$)	Errors in ζ
ζ_1	$x_1(t)$	0.10	2.6427	2.6506	0.30%
	$x_2(t)$	0.10	2.6275	2.6506	0.90%
ζ_2	$x_1(t)$	0.26	1.1187	1.1507	2.78%
	$x_2(t)$	0.26	1.1452	1.1507	0.47%

From **Tables 7** and **8**, it can be observed that for the new system with a higher damping ratio, the maximum computational error is 2.78% and the minimum is 0.30%. This demonstrates the applicability of the filter-based method to such systems. Furthermore, when the errors of the high-damping system are compared with those of the low-damping system (**Tables 2** and **5**), they are found to be numerically similar. This indicates that the method achieves comparable accuracy for both cases. Overall, the filter-based method provides a high level of computational accuracy and is applicable to 2DOF systems with either high or low damping ratios.

In practical applications, FRFs are typically derived from real-world data, where measurement noise can significantly influence the results. This noise can introduce inaccuracies in the estimation of damping ratios and modal parameters. To mitigate these effects, techniques such as noise filtering, statistical averaging, and robust estimation can be employed.

3. HQGM and its improvement

3.1. Original HQGM for SDOF systems

The dynamic equation of a SDOF system shown in **Figure 8a** can be written as [26].

$$m\ddot{x}(t) + c\dot{x}(t) + kx(t) = F(t)) \tag{20}$$

where m, c, and k denote the mass, viscous damping coefficient, and stiffness of the system, respectively; x, $\dot{x}$, and $\ddot{x}$ represent displacement, velocity, and acceleration. The variable t denotes time, and $F(t)$ is the external excitation force. The Half-Quadratic Gain Method is based on the analysis of FRF of an SDOF system. The FRF is obtained either by taking the ratio of the Fourier transforms between the output and input signals. This approach is straightforward, being suitable for systems with deterministic or periodic excitations. Subsequently, the relationship between the squared magnitude of the FRF and the excitation frequency f is established.

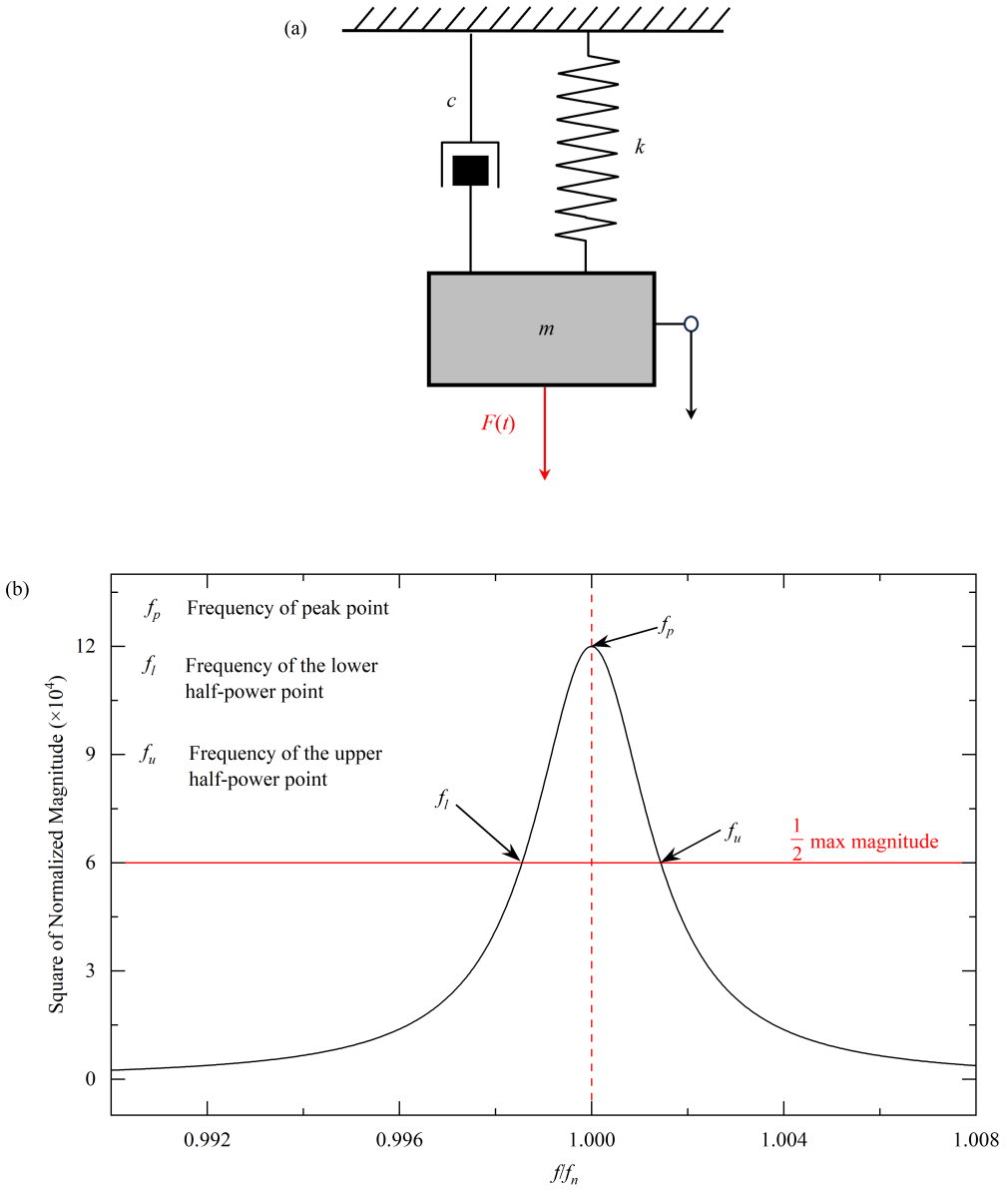

Figure 8. **(a)** Forced vibration of a SDOF system; **(b)** Normalized magnitude squared curve of FRF in a SDOF system.

Figure 8b illustrates this relationship for the SDOF system. The peak of the squared FRF magnitude can be identified at f_p. Next, the two frequencies at which the squared magnitude drops to half of the peak value can be determined, referred to as the half-power points. These frequencies are denoted as the lower half-power frequency f_l and the upper half-power frequency f_u.

The damping ratio of the system is related to the peak frequency and the frequencies of the half-power points [6]. The relationship of the damping ratio with the three frequencies (f_l, f_p, and f_u) is:

$$\zeta = \sqrt{\frac{1}{2} - \sqrt{\left(4 + 4\left(\frac{f_u - f_l}{f_p}\right)^2 - \left(\frac{f_u - f_l}{f_p}\right)^4\right)^{-1}}} \tag{21}$$

It is an exact formula for calculating the damping ratio of an excited SDOF system.

The Half-Quadratic Gain Method is closely related to the concept of the quality factor (Q-factor) in vibratory systems. Both approaches involve analyzing the FRF of a SDOF system. Both methods use the squared magnitude of the FRF to identify the peak frequency and the half-power points, which are essential for determining system damping or quality factor.

3.2. Direct application to MDOF systems

Consider the 2DOF excited system introduced in Section 2.2. The equations of motion for this system are already given in Equation (12). The explicit forms of the mass matrix, damping matrix, stiffness matrix, and external force vector are presented below.

$$M = \begin{pmatrix} m_1 & 0 \\ 0 & m_2 \end{pmatrix} \tag{22}$$

$$C = \begin{pmatrix} c_1 & 0 \\ 0 & c_2 \end{pmatrix} \tag{23}$$

$$K = \begin{pmatrix} k_1 + k_2 & -k_2 \\ -k_2 & k_2 \end{pmatrix} \tag{24}$$

$$F(t) = \begin{pmatrix} F_1 sin\left(\omega_1 t + \varphi_1\right) \\ F_2 sin\left(\omega_2 t + \varphi_2\right) \end{pmatrix} \tag{25}$$

In the frequency domain, the equation of motion of the system is:

$$\left(-M\omega^2 + iC\omega + K\right) X(\omega) = F(\omega) \tag{26}$$

where $X(\omega)$ is the displacement response vector, containing the response of two degrees of freedom, $F(\omega)$ is the force vector, and each component corresponds to a frequency-domain representation of the force.

The FRF, denoted by $H(\omega)$, is defined as the ratio of the system output to its input in the frequency domain. The relationship between the output X (ω) and the input $F(\omega)$

is:

$$X(\omega) = H(\omega)F(\omega) \tag{27}$$

Therefore, the FRF matrix $H(\omega)$ is:

$$H(\omega) = \left(-M\omega^2 + iC\omega + K\right)^{-1} \tag{28}$$

For the 2DOF system, the FRF is a matrix:

$$H(f) = \begin{pmatrix} H_{11}(f) & H_{12}(f) \\ H_{21}(f) & H_{22}(f) \end{pmatrix} \tag{29}$$

where $H_{11}(f)$ denotes the response of mass 1 under the excitation force F_1, and $H_{22}(f)$ denotes the response of mass 2 under the excitation force F_2. The term $H_{12}(f)$ represents the response of mass 1 due to F_2 applied at mass 2, transmitted through the dynamic coupling between the two masses. Similarly, $H_{21}(f)$ represents the response of mass 2 due to F_1 applied at mass 1, also induced by the coupling effect.

Therefore, $H_{11}(f)$ and $H_{22}(f)$ are referred to as self-response functions, as they characterize the response of each degree of freedom to its own excitation. In contrast, $H_{12}(f)$ and $H_{21}(f)$ are referred to as mutual response functions as they capture the coupling effect between the two degrees of freedom; specifically, how the excitation applied to one degree of freedom influences the response of the other.

The key to estimating the system's damping ratio in HQGM lies in accurately determining the FRF. From Equation (28), it can be seen that the system's FRF depends only on the system's mass, damping, and stiffness. However, in practical applications, information such as the system's damping and stiffness is often difficult to obtain. Nevertheless, according to Equation (27), the system's FRF can also be determined from the external force applied to the system and the resulting displacement. Therefore, in this study, when applying the HQGM method to estimate the damping ratio of the case system, only the excited vibration scenario is considered, while the free vibration case is not taken into account.

In SDOF systems, no coupling effects exist, and the calculation of the damping ratio is relatively straightforward. In contrast, in MDOF systems, the response of each degree of freedom is influenced not only by its own external excitation but also by interactions with the rest of the system. Such coupling effects introduce considerable complexity into the estimation of damping ratios. For example, when applying the HQGM, modal coupling can lead to overlapping or distortion of resonance peaks, thereby altering their characteristics and potentially affecting the accuracy of the results. To assess the extent to which modal coupling influences damping ratio estimation using HQGM in MDOF systems, the 2DOF system in Section 2.2 is analyzed. The damping ratio is first calculated directly using the HQGM, and the resulting computational errors are then examined.

For the 2DOF system presented in **Figure 5a**, the FRF of the system is shown in **Figure 9**. The mutual response functions $|H_{12}(f)|$ and $|H_{21}(f)|$ exhibit significant peak amplitudes at frequencies corresponding to the primary resonance peaks of the

self-response functions $|H_{11}(f)|$ and $|H_{22}(f)|$, respectively. Specifically, at the frequency where $|H_{11}(f)|$ attains its maximum, $|H_{12}(f)|$ reaches approximately 15% of the peak amplitude of $|H_{11}(f)|$. Similarly, at the frequency corresponding to the peak of $|H_{22}(f)|$, $|H_{21}(f)|$ attains nearly 67% of the peak amplitude of $|H_{22}(f)|$. These pronounced peaks in the mutual response functions suggest a coupling effect between the two degrees of freedom, indicating that the modes are not independent but instead exhibit considerable dynamic interaction.

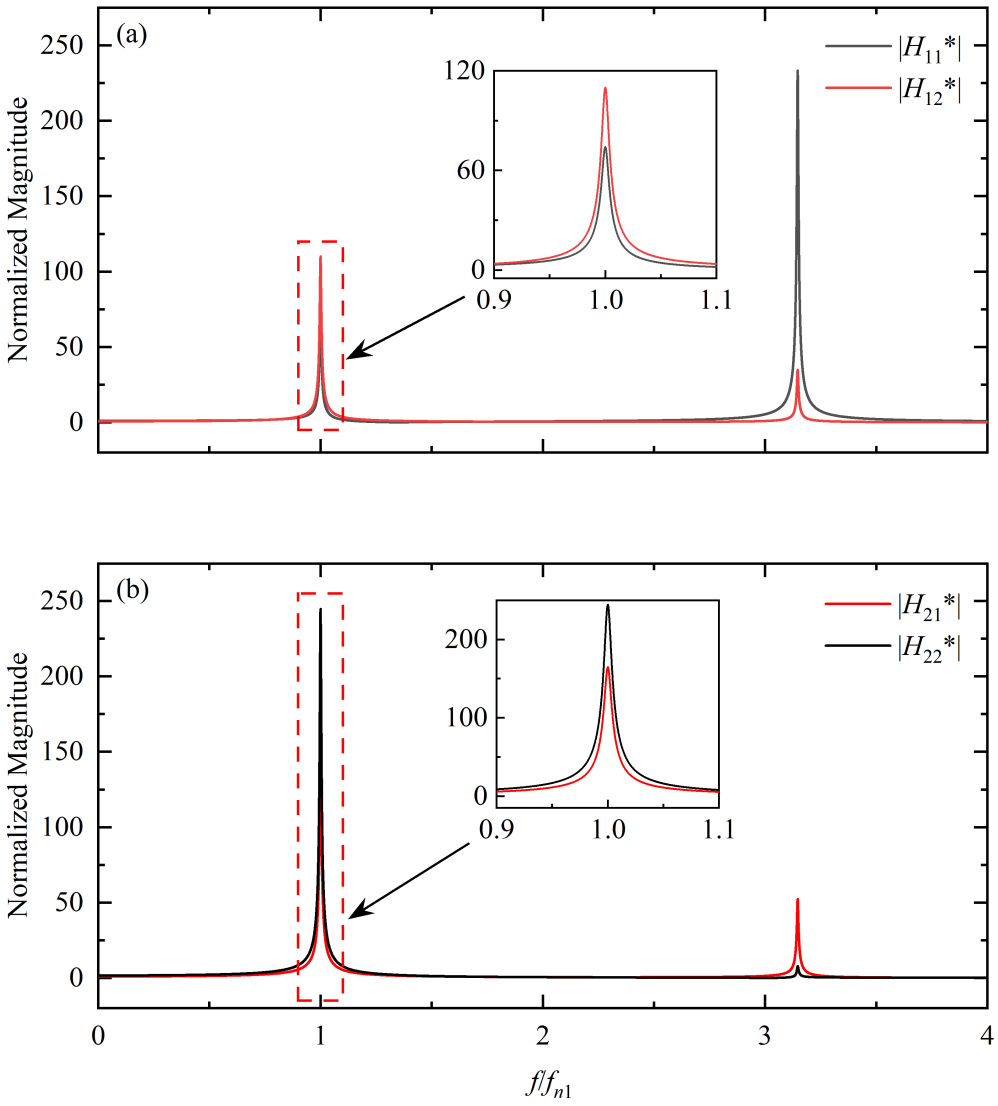

Figure 9. Normalized magnitude curves: **(a)** $H_{11}(f)$ and $H_{12}(f)$; **(b)** $H_{21}(f)$ and $H_{22}(f)$.

In a typical 2DOF system, two distinct natural frequencies correspond to two vibration modes. As shown in **Figure 9**, each self-response function exhibits two resonance peaks: one at a lower frequency and one at a higher frequency. The height of each peak indicates the amplitude of response at resonance, while the square of the amplitude is proportional to the energy associated with that response.

To estimate the damping ratios of the individual modes using the HQGM, it is essential to analyze the squared magnitude curves of FRF. However, a critical question arises regarding which resonance peaks should be selected for the damping ratio calculation among the eight available peaks. From a physical standpoint, the

self-response functions $H_{11}(f)$ and $H_{22}(f)$ are expected to provide the most reliable damping information. This is because $H_{11}(f)$ represents the response at location 1 due to excitation at the same location, which directly reflects the local dynamic characteristics with minimal cross-coupling interference. In the modal expansion, when a particular mode has strong participation at a specific location, the corresponding resonance peak is dominated by that mode's inherent damping properties.

Among the two peaks in each self-response function, the peak with higher magnitude is expected to provide more accurate damping estimates, as higher peaks indicate stronger modal participation and better signal-to-noise ratios. To validate these theoretical considerations, the HQGM is systematically applied to all eight resonance peaks across the four FRFs. The results and the error using HQGM directly are shown in **Table 9**. The results in **Table 9** validate the theoretical predictions regarding the selection of appropriate FRFs for damping ratio estimation. The eight resonance peaks were categorized into two groups based on their frequencies for comparative analysis: peaks at 1.17 Hz corresponding to the first mode, and peaks at 3.70 Hz corresponding to the second mode. Within each frequency group, the four FRFs ($H_{11}(f)$, $H_{12}(f)$, $H_{21}(f)$, $H_{22}(f)$) were compared in terms of damping ratio estimation accuracy. The analysis reveals that at 1.17 Hz, $H_{22}(f)$ exhibits the smallest calculation error among the four functions, with this peak coincidentally being the dominant peak of $H_{22}(f)$. Similarly, at 3.70 Hz, $H_{11}(f)$ demonstrates the highest accuracy, where this peak happens to be the dominant peak of $H_{11}(f)$. The results strongly support the proposed approach of utilizing the dominant resonance peaks of $H_{11}(f)$ and $H_{22}(f)$ as the optimal choice for damping ratio calculation in 2DOF systems.

Table 9. Errors in the system using the Half-Quadratic Gain Method directly.

FRFs	Frequencies (Hz)	Estimated ζ_e ($\times 10^{-3}$)	Actual ζ_a ($\times 10^{-3}$)	Errors
$H_{11}(f)$	1.17	3.36994	3.36943	0.01514%
	3.70	1.07092	1.07093	0.00093%
$H_{12}(f)$	1.17	3.37035	3.36943	0.02730%
	3.70	1.07110	1.07093	0.01587%
$H_{21}(f)$	1.17	3.36974	3.36943	0.00920%
	3.70	1.07075	1.07093	0.01681%
$H_{22}(f)$	1.17	3.36933	3.36943	0.00297%
	3.70	1.07266	1.07093	0.16154%

The comprehensive evaluation across all eight resonance peaks reveals that the maximum error when applying the HQGM to this 2DOF system is merely 0.16%. This low error margin demonstrates that the direct application of the HQGM to the selected 2DOF system yields acceptable accuracy for practical engineering applications. While coupling effects are evident from the FRF plots, the unexpectedly small calculation errors suggest that the coupling strength in this particular system may be relatively weak, allowing the HQGM to maintain its effectiveness despite being originally developed for SDOF systems. The modal damping ratios of approximately 0.00107 and 0.00337 represent light damping conditions, under which the method demonstrates satisfactory performance for this specific system configuration.

3.3. Improved HQGM for MDOF systems

While the direct application of HQGM to the 2DOF system introduced in Section 2.2 demonstrated satisfactory accuracy, the presence of coupling effects inevitably influences the precision of damping ratio calculations. The coupling between degrees of freedom introduces cross-modal interference that can distort the frequency response characteristics, potentially affecting the identification of pure modal parameters. Therefore, this section presents an improved HQGM approach specifically designed to reduce the impact of coupling effects in MDOF systems. The objective is to enhance the method's computational precision and extend its applicability to more complex dynamic systems.

The improvement strategy is inspired by the frequency response characteristics of SDOF systems. In SDOF systems, the FRF exhibits a single resonance peak corresponding to the system's natural frequency. For uncoupled 2DOF systems, the self-response functions $H_{11}(f)$ and $H_{22}(f)$ would theoretically display only one resonance peak each, analogous to independent SDOF systems. However, in coupled systems, the presence of coupling effects results in both $H_{11}(f)$ and $H_{22}(f)$ exhibiting two distinct peaks: a dominant peak and a secondary peak. This observation leads to a conceptual approach for improving the HQGM accuracy. If a method could be developed to eliminate the secondary peaks from $H_{11}(f)$ and $H_{22}(f)$, leaving only the dominant peak in each function, the resulting frequency response would resemble that of a SDOF system. Such a modification would theoretically eliminate the influence of coupling effects, thereby enabling more accurate damping ratio calculations using the original HQGM formulation.

The elimination of secondary peaks in self-response functions is achieved through a straightforward modification approach that leverages the coupling information embedded in mutual response functions. The mutual response functions $H_{12}(f)$ and $H_{21}(f)$ inherently contain the coupling characteristics of the system, as they represent the dynamic transmission between different degrees of freedom. To develop a practical and efficient correction method suitable for engineering applications, this study proposes a modification formula based on complex-domain subtraction with adjustable coefficients. The modified self-response functions are obtained by subtracting a proportional amount of the corresponding mutual response functions from the original self-response functions:

$$\begin{aligned} H_{11}(f)_{\text{corrected}} &= H_{11}(f) - rH_{12}(f) \\ H_{22}(f)_{\text{corrected}} &= H_{22}(f) - r^{'}H_{21}(f) \end{aligned} \tag{30}$$

where r and $r^{'}$ are system-dependent correction coefficients that need to be determined based on the specific characteristics of each system. The correction is performed directly on the complex-valued FRFs rather than their magnitudes, ensuring that both amplitude and phase information are preserved throughout the process. Depending on the phase relationships between the self-response and mutual response functions, the correction coefficients may assume negative values, which naturally accounts for the directional effects of coupling. This approach offers significant advantages in

terms of implementation simplicity, as it directly utilizes the coupling information contained within the mutual response functions without requiring complex modal decomposition. The objective is to obtain modified self-response functions whose magnitude plots exhibit a single dominant resonance peak, similar to the frequency response characteristics of SDOF systems. An initial value range is first estimated. The correction factor is then varied uniformly within this range, and FRF curves are generated for the sampled values. The correction factor producing the strongest suppression of the secondary peak is identified, and a narrower range is subsequently defined. This procedure is repeated until the secondary peak is nearly eliminated, at which point the optimal correction factor is obtained. The assumption that removing secondary peaks in the self-response functions eliminates coupling effects is valid for linear, weakly coupled systems. However, in real-world systems with more complex coupling or nonlinear damping, this assumption may not hold.

From Equation (30), it is known that the determination of the correction factor r is based solely on the characteristics of $H_{11}(f)$ and $H_{12}(f)$, independent of $H_{22}(f)$ and $H_{21}(f)$. From **Figure 9**, it is observed that $H_{11}(f)$ has its dominant peak at 3.70 Hz and a secondary peak at 1.17 Hz. Therefore, this analysis focuses on the frequency range around 1.17 Hz. As shown in **Figure 10**, when r varies from 0.1 to 1.0, the magnitude of the secondary peak initially decreases and then increases, reaching local minima at $r = 0.4$ and $r = 0.5$. This indicates that the optimal correction factor likely lies within this interval. A closer examination of the responses within this range further reveals that the secondary peak attains its minimum when $r = 0.45$, at which point the curve becomes nearly flat around 1.17 Hz. Based on this analysis, the optimal value of the correction factor is determined to be $r = 0.45$.

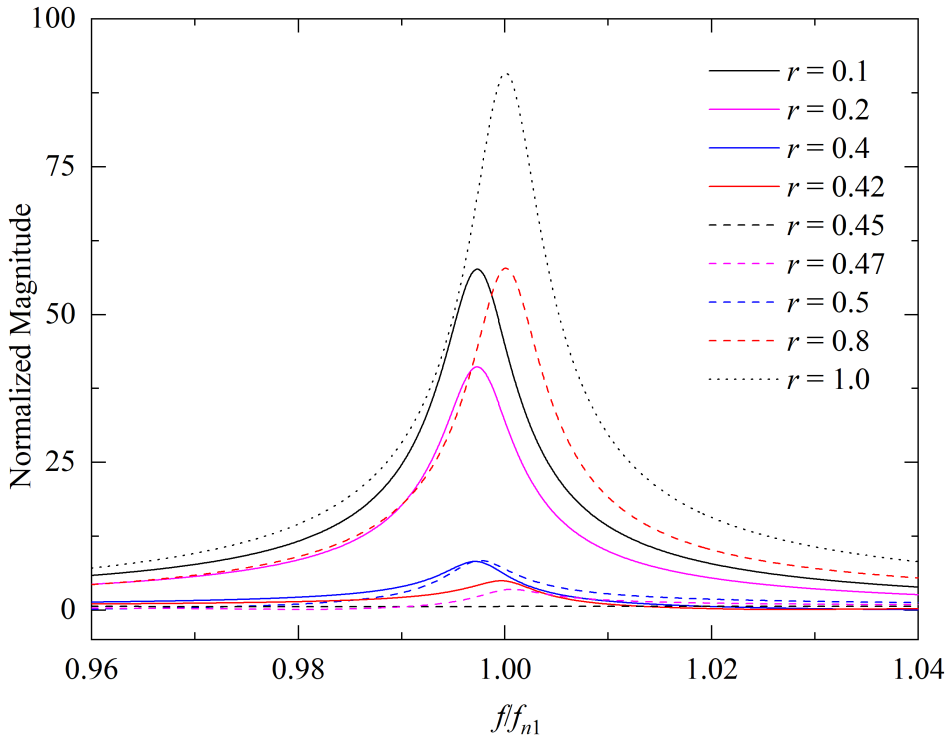

Figure 10. Magnitude curves of corrected $H_{11}(f)$ under varying correction factors r for suppression of the secondary peak.

A similar procedure is employed to determine the correction factor r'. **Figure 11** reveals that when $r' = -0.22$, the magnitude curve of the corrected $H_{22}(f)$ achieves its lowest secondary peak at 3.70 Hz. At this value, the curve becomes nearly flat in the vicinity of the target frequency, confirming that $r' = -0.22$ is the most appropriate correction factor.

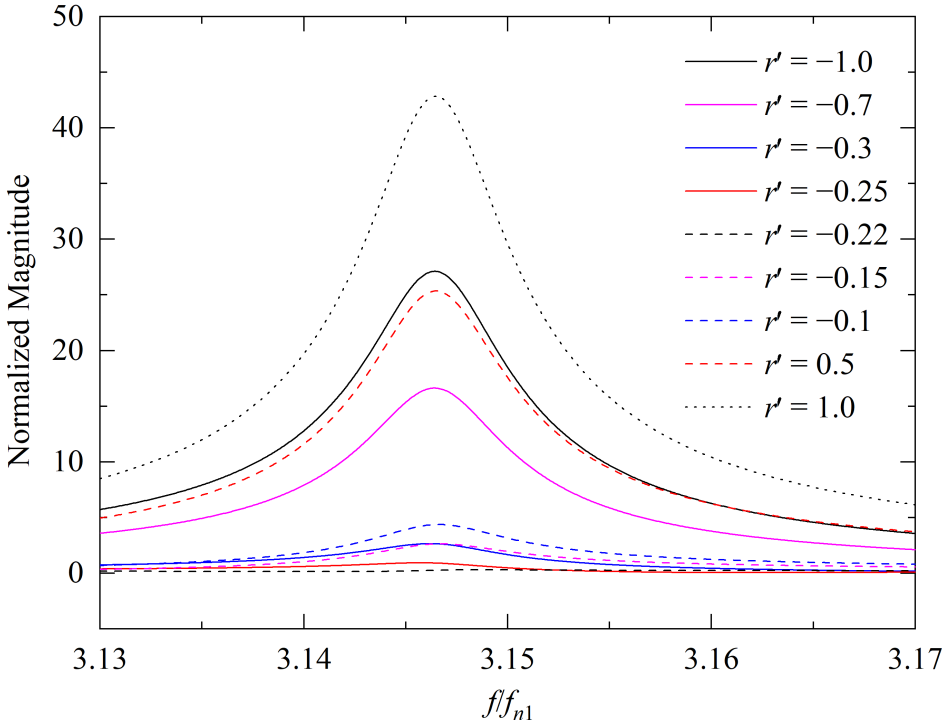

Figure 11. Magnitude curves of corrected $H_{22}(f)$ under varying correction factors r' for suppression of the secondary peak.

With the optimal values of $r = 0.45$ and $r' = -0.22$ determined, the correction formulas are fully defined. **Figure 12** compares the magnitude profiles of the original and corrected self-response functions. The corrected responses clearly show a single dominant resonance peak in each function, consistent with the behavior of a weakly coupled system.

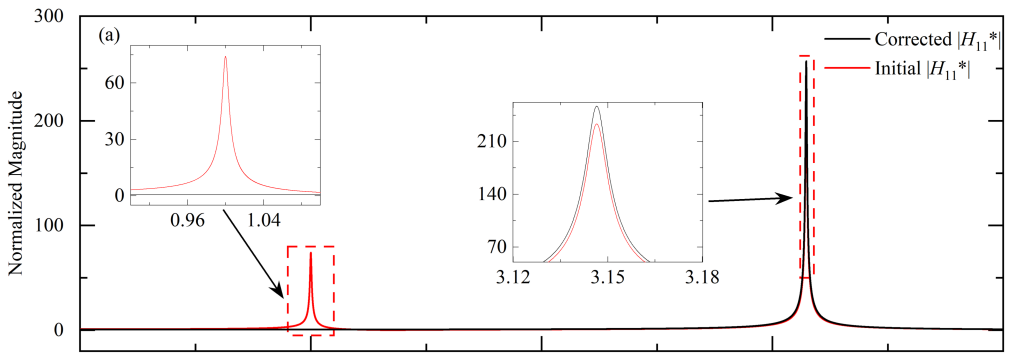

Figure 12. *Cont.*

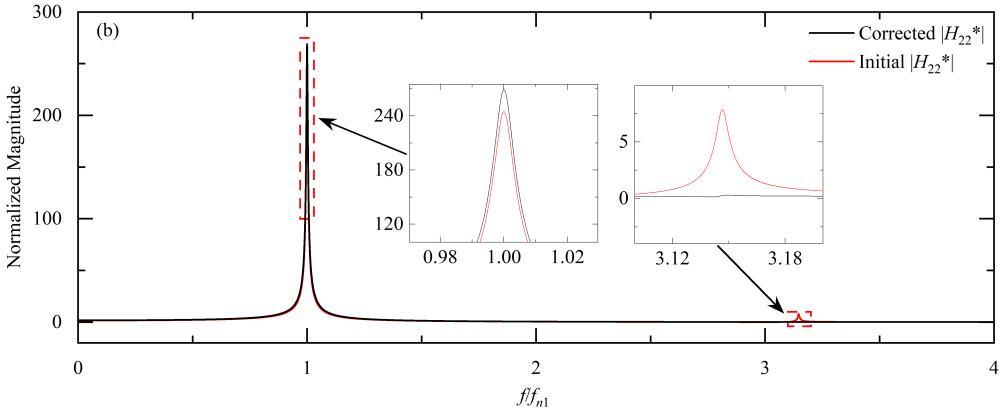

Figure 12. Comparison of normalized magnitude of **(a)** $H_{11}(f)$; **(b)** $H_{22}(f)$ before and after corrected.

After obtaining the corrected self-response functions $H_{11}(f)$ and $H_{22}(f)$, the HQGM is applied to estimate the modal damping ratios. For the 2DOF system described in Section 2.2, the computed damping ratios and their corresponding errors using the improved HQGM are summarized in **Table 10**.

Table 10. Errors in the system using the improved HQGM.

FRFs	Frequencies (Hz)	Estimated ζ_e ($\times 10^{-3}$)	Actual ζ_a ($\times 10^{-3}$)	Errors
$H_{11}(f)$	3.70	1.07107	1.07093	0.01307%
$H_{22}(f)$	1.17	3.37009	3.36943	0.01959%

The results of applying the improved HQGM to the 2DOF system demonstrate acceptable accuracy, with a maximum error not exceeding 0.02%, which falls within the range suitable for practical engineering applications. However, comparison between **Tables 9** and **10** reveals that the improved method produces larger calculation errors than the original HQGM when applied to the same system. When using the dominant peaks of H_{11} and H_{22}, the original method exhibits errors that are two and one orders of magnitude smaller, respectively, than those of the improved approach. These results indicate that for this particular system, the improved HQGM does not provide the anticipated enhancement in accuracy. A plausible explanation is that the coupling strength between the two degrees of freedom in this system is relatively weak, making the original method more suitable for such weakly coupled conditions, while the improved HQGM may demonstrate advantages only in systems with stronger coupling characteristics.

3.4. Damping estimation in a strongly coupled system

The analysis of results in the previous section reveals that the improved HQGM did not outperform the original method for the investigated system, prompting further examination of the method's applicability range. To test the hypothesis that the improved HQGM may be more effective for strongly coupled systems, this section investigates a 2DOF system with significantly enhanced coupling characteristics. The objective is to determine whether the proposed modification demonstrates superior performance when coupling effects are more pronounced, thereby establishing the

appropriate application scope for each method.

The new system's parameters are as follows: m_1 = 6 kg, m_2 = 5 kg, c_1 = 0.05 Nm/s, c_2 = 0.08 Nm/s, k_1 = 1200 N/m, k_2 = 1000 N/m. The magnitude profile of the corresponding FRF is shown in **Figure 13**.

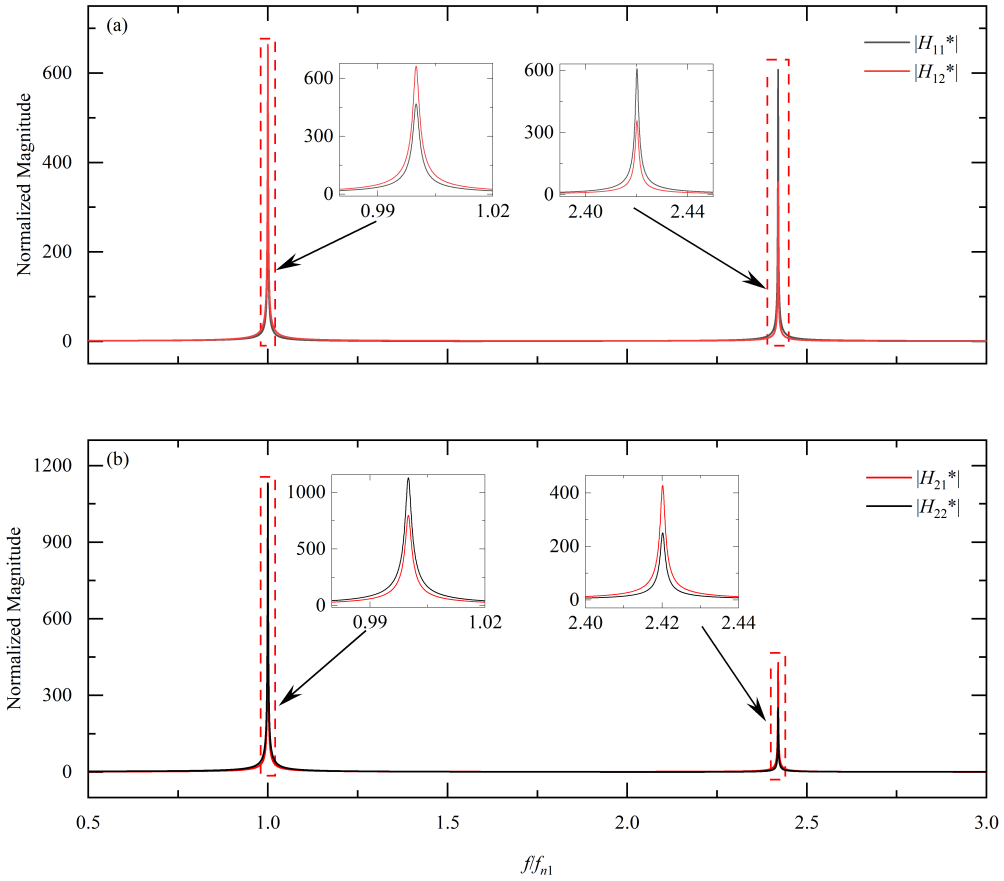

Figure 13. Normalized magnitude responses in new system: **(a)** $H_{11}(f)$ and $H_{12}(f)$; **(b)** $H_{21}(f)$ and $H_{22}(f)$.

To assess the relative coupling characteristics between the newly designed system and the original system, a comparative analysis is performed based on the FRF features. The magnitude ratio between the secondary peak and the dominant peak in the self-response functions serves as an indicator of coupling strength, with higher ratios suggesting stronger coupling effects. **Table 11** presents the magnitude ratios of secondary-to-dominant peaks for both systems, providing a quantitative basis for this qualitative comparison.

Table 11. Magnitude ratio of secondary to dominant peak in FRF (old vs. new system).

System	FRF	Dominant peak frequency (Hz)	Dominant peak magnitude	Secondary peak frequency (Hz)	Secondary peak magnitude	Ratio
Original	$H_{11}(f)$	3.70	233.43	1.17	74.20	31.79%
New	$H_{11}(f)$	3.50	607.78	1.47	467.53	76.92%
Original	$H_{22}(f)$	1.17	244.82	3.70	7.86	3.21%
New	$H_{22}(f)$	1.47	1131.5	3.50	251.12	22.19%

As shown in **Table 11**, the newly designed system exhibits significantly higher secondary-to-dominant peak ratios compared to the original system, indicating stronger

coupling characteristics. To evaluate the performance of both methods under these enhanced coupling conditions, the same analytical procedures applied to the original system are now implemented on the new system. Specifically, both the original HQGM and the improved HQGM are employed to calculate the modal damping ratios, and the resulting errors are compared to assess the effectiveness of each method in the presence of stronger coupling. The calculation results are presented in **Tables 12** and **13**.

Table 12. Errors in the new system using the HQGM directly.

	Frequencies (Hz)	**Estimated ζ ($\times 10^{-4}$)**	**Actual ζ ($\times 10^{-4}$)**	**Errors**
$H_{11}(f)$	3.50	2.409853	2.409025	0.037365%
$H_{22}(f)$	1.47	7.569766	7.590172	0.268853%

Table 13. Errors in the new system using the improved HQGM.

	Frequencies (Hz)	**Estimated ζ ($\times 10^{-4}$)**	**Actual ζ ($\times 10^{-4}$)**	**Errors**
$H_{11}(f)$	3.50	2.409481	2.409025	0.018923%
$H_{22}(f)$	1.47	7.570699	7.590172	0.256561%

The calculation results reveal a significant finding: for the newly designed system with stronger coupling characteristics, the improved HQGM demonstrates superior performance compared to the original method. As shown in **Tables 12** and **13**, the improved HQGM consistently produces smaller errors when calculating damping ratios using both the dominant peak of $H_{11}(f)$ and the dominant peak of $H_{22}(f)$. This outcome validates the hypothesis proposed earlier and suggests that the improved HQGM is indeed more suitable for systems with stronger coupling effects. The correction approach, which removes coupling-induced secondary peaks through complex-domain subtraction, effectively enhances the accuracy of damping ratio estimation when coupling between degrees of freedom becomes significant.

In summary, this section investigated the applicability of the improved HQGM by designing a system with enhanced coupling characteristics. Through comparative analysis of FRF features, it is confirmed that the new system exhibits stronger coupling than the original system, as evidenced by the higher secondary-to-dominant peak ratios in the self-response functions. Both the original and improved HQGM were applied to this strongly coupled system, and the results demonstrate that the improved method achieves better accuracy in damping ratio calculations. These findings establish that while the original HQGM may be sufficient for weakly coupled systems, the improved HQGM provides distinct advantages when dealing with systems where coupling effects are more pronounced. This clarifies the appropriate application scope for each method and provides practical guidance for selecting the suitable approach based on system coupling characteristics. A computational flowchart summarizing the proposed improved HQGM is presented in **Figure 14**.

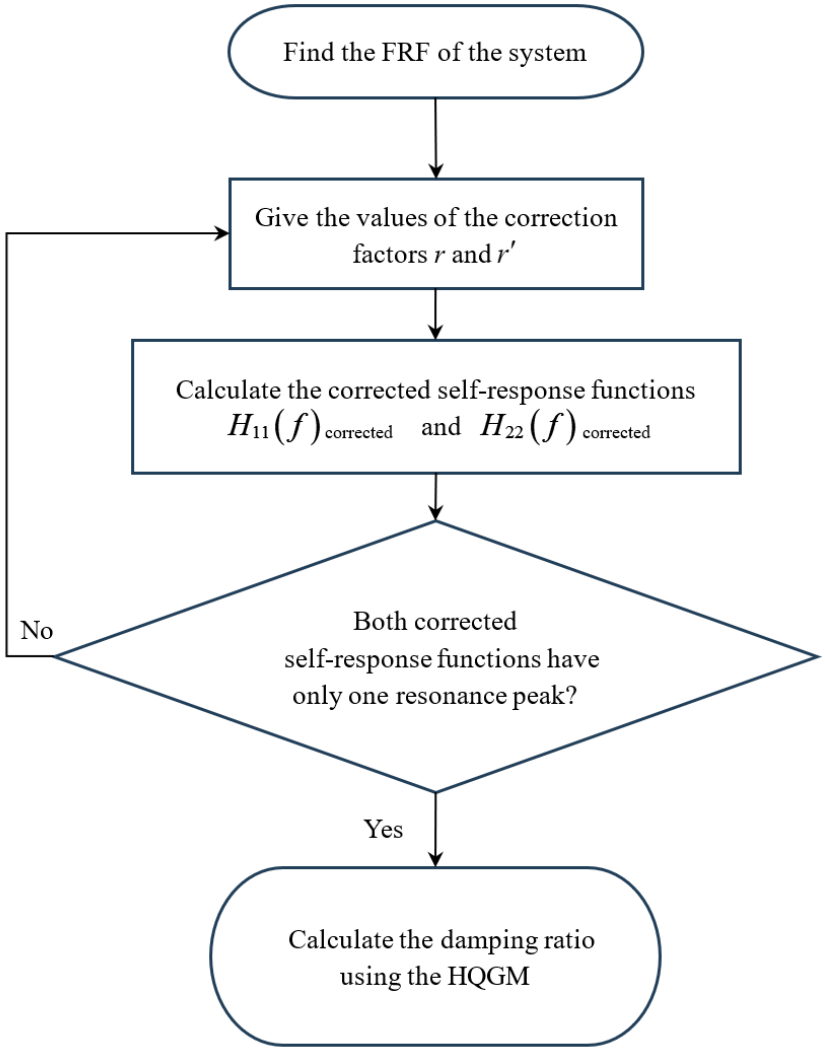

Figure 14. Computational flowchart of the improved HQGM.

4. Conclusion

This study presents two approaches for estimating damping ratios in multi-degree-of-freedom (MDOF) systems: a filter-based method and an improved Half-Quadratic Gain Method (HQGM). The performance of each technique is examined across different system configurations, including unexcited and excited 2DOF systems as well as systems with low and high damping ratios and varying coupling strengths.

The filter-based method demonstrates robust performance by accurately extracting modal decay characteristics directly from vibration displacement signals. Through envelope fitting and logarithmic analysis, it achieves damping ratio predictions with errors consistently below 3% for both low- and high-damping cases, confirming its broad applicability and reliability. The method, grounded in theoretical foundations and supported by numerical validation, demonstrates effectiveness even under forced excitation, confirming its potential for practical engineering systems where direct measurement of damping and stiffness is challenging.

The HQGM, initially designed for SDOF systems, is successfully extended to MDOF systems. When applied directly to weakly coupled systems, the original

HQGM produces highly accurate damping estimates, with errors not exceeding 0.16%. However, for strongly coupled systems, coupling effects lead to interference between resonance peaks, reducing accuracy. To address this, an improved HQGM is proposed, introducing a correction formula based on complex-domain subtraction of mutual response functions. This modification effectively suppresses coupling-induced secondary peaks, restoring SDOF-like frequency response characteristics. The improved HQGM achieved superior accuracy in strongly coupled systems, reducing estimation errors compared to the original method.

Overall, the findings can be pointed out as follows:

1. The filter-based method provides a simple, efficient, and accurate technique for determining damping ratios in both free and forced vibration systems, regardless of damping magnitude.
2. The original HQGM performs best in weakly coupled systems, offering very high accuracy.
3. The improved HQGM enhances performance for strongly coupled systems by mitigating cross-modal interference and achieving higher precision.
4. Both methods are suitable for practical structural applications where modal parameters are difficult to obtain experimentally.

These methods provide a reliable and cost-effective alternative to traditional experimental techniques, making them highly applicable in real-world scenarios where access to experimental setups is limited or infeasible. The ability to estimate damping ratios and modal parameters directly from numerical simulations can greatly enhance the analysis of structural systems, particularly in cases involving complex geometries or inaccessible experimental conditions. While the current study focuses on linear systems, real-world applications often involve systems with varying parameters, and these variations may lead to errors in damping estimation. Further research is necessary to explore methods that can account for nonlinearities and system parameter fluctuations, improving the method's applicability in more complex scenarios.

While the proposed approaches have demonstrated excellent performance in 2DOF systems, generalization to systems with three or more degrees of freedom presents additional challenges, such as more complex correction formulations and the need to determine multiple correction factors. Future work is required to further validate these techniques through experimental data and real-world case studies.

Author contributions: Conceptualization, MMA; methodology, FC and MMA; software, MMA and FC; validation, MMA, FC, VT and CJ; formal analysis, FC, MMA and HZ; investigation, FC and MMA; resources, MMA, TC, and HZ; data curation, FC, CJ, and VT; writing—original draft preparation, FC and MMA; writing—review and editing, MMA, HZ, CJ, MZ, TC, and VT; visualization, FC; supervision, MMA; project administration, MMA; funding acquisition, MMA. All authors have read and agreed to the published version of the manuscript.

Funding: This work was supported by NSFC grant number 11672096.

Institutional review board statement: Not applicable.

Informed consent statement: Not applicable.

Data availability statement: The data presented in this study are available on request from the corresponding author

Conflict of interest: The authors declare no conflict of interest.

Abbreviation

M	mass matrix
C	damping matrix
K	stiffness matrix
X	displacement of the system
$\dot{X}$	velocity of the system
$\ddot{X}$	acceleration of the system
M	mass of the system
C	damping of the system
K	stiffness of the system
A	decay factor
B	damped natural frequency
ζ	damping ratio
f_n	undamped natural frequency
F	excitation force
f_p	peak of the squared FRF magnitude
f_l	lower half-power frequency
f_u	upper half-power frequency
$H(f)$	frequency response function
R	the first correction coefficient
r'	the second correction coefficient

References

1. Cheynet E, Jakobsen JB, Snæbjörnsson J. Damping estimation of large wind-sensitive structures. Procedia Engineering. 2017; 199: 2047–2053. doi: 10.1016/j.proeng.2017.09.471
2. Peng S, Alam MM, Zhou Y. Fluid-structure interaction of a fixed-fixed high-aspect-ratio flexible wing in crossflow. Journal of Fluids and Structures. 2026; 141: 104486. doi: 10.1016/j.jfluidstructs.2025.104486
3. Li Z, Li P, Jiang Z, et al. Difference of bridge damping ratio under different excitations. Journal of Vibration and Shock. 2016; 35(3): 62–67.
4. Bhatt R, Alam MM. Vibrations of a square cylinder submerged in a wake. Journal of Fluid Mechanics. 2018; 853: 301–332. doi: 10.1017/jfm.2018.573
5. Lin C, Alam MM. Intrinsic features of flow-induced stability of a square cylinder. Journal of Fluid Mechanics. 2024; 988: A50. doi: 10.1017/jfm.2024.445
6. Casiano MJ. Extracting Damping Ratio from Dynamic Data and Numerical Solutions. NASA Marshall Space Flight Center; 2016.
7. Naylor S, Platten MF, Wright JR, et al. Identification of Multi-Degree of Freedom Systems with Nonproportional Damping Using the Resonant Decay Method. Journal of Vibration and Acoustics. 2004; 126(2): 298–306. doi: 10.1115/1.1687395
8. Meo M, Zumpano G, Meng X, et al. Measurements of dynamic properties of a medium span suspension bridge by using the wavelet transforms. Mechanical Systems and Signal Processing. 2006; 20(5): 1112–1133. doi:

10.1016/j.ymssp.2004.09.008
9. Wang Z, Zhai F. The identification method of damping ratio of closely-space MDOF system using analytic wavelet. Journal of Qingdao University of Science and Technology (Natural Science Edition). 2006; 27(4): 347–351.
10. Ku CJ, Cermak JE, Chou L-S. Random decrement based method for modal parameter identification of a dynamic system using acceleration responses. Journal of Wind Engineering and Industrial Aerodynamics. 2007; 95(6): 389–410. doi: 10.1016/j.jweia.2006.08.004
11. He XH, Hua XG, Chen ZQ, et al. EMD-based random decrement technique for modal parameter identification of an existing railway bridge. Engineering Structures. 2011; 33(4): 1348–1356. doi: 10.1016/j.engstruct.2011.01.012
12. Yang XM, Yi TH, Qu CX, et al. Modal Identification of High-Speed Railway Bridges through Free-Vibration Detection. Journal of Engineering Mechanics. 2020; 146(9): 04020107. doi: 10.1061/(ASCE)EM.1943-7889.0001847
13. Dan D, Yu X, Han F, et al. Research on dynamic behavior and traffic management decision-making of suspension bridge after vortex-induced vibration event. Structural Health Monitoring. 2022; 21(3): 872–886. doi: 10.1177/14759217211011582
14. Niu Y, Ye Y, Zhao W, et al. Identifying Modal Parameters of a Multispan Bridge Based on High-Rate GNSS–RTK Measurement Using the CEEMD–RDT Approach. Journal of Bridge Engineering. 2021; 26(8): 04021049. doi: 10.1061/(ASCE)BE.1943-5592.0001754
15. Hallal J, Fakih M, Damerji H, et al. Experimental Modal Damping Identification of a Mechanical Structure Using Video Magnification Technique. Sound & Vibration. 2021; 55(2): 131–140. doi: 10.32604/sv.2021.015293
16. Tsatsas I, Pontillo A, Lone M. Aeroelastic Damping Estimation for a Flexible High-Aspect-Ratio Wing. Journal of Aerospace Engineering. 2022; 35(2): 04021135. doi: 10.1061/(ASCE)AS.1943-5525.0001390
17. Olmos BA, Roesset JM. Evaluation of the half-power bandwidth method to estimate damping in systems without real modes. Earthquake Engineering & Structural Dynamics. 2010; 39(14): 1671–1686. doi: 10.1002/eqe.1010
18. López-Aragón JA, Puchol V, Astiz MA. Influence of the modal damping ratio calculation method in the analysis of dynamic events obtained in structural health monitoring of bridges. Journal of Civil Structural Health Monitoring. 2024; 14(5): 1191–1213. doi: 10.1007/s13349-023-00760-y
19. Lee TS, Ooi EH, Chang WS, et al. Fractal grid-induced turbulence strength characterization via piezoelectric thin-film flapping velocimetry. Scientific Reports. 2021; 11(1): 23322. doi: 10.1038/s41598-021-02680-7
20. Liu Q, Wang Y, Sun P, et al. Comparative Analysis of Viscous Damping Model and Hysteretic Damping Model. Applied Sciences. 2022; 12(23): 12107. doi: 10.3390/app122312107
21. Köhler A, Ohrnberger M, Scherbaum F, et al. Assessing the reliability of the modified three-component spatial autocorrelation technique. Geophysical Journal International. 2007; 168(2): 779–796. doi: 10.1111/j.1365-246X.2006.03253.x
22. Qin B, Alam MM, Zhou Y. Two tandem cylinders of different diameters in cross-flow: Flow-induced vibration. Journal of Fluid Mechanics. 2017; 829: 621–658. doi: 10.1017/jfm.2017.510
23. Qin B, Alam MM, Zhou Y. Free vibrations of two tandem elastically mounted cylinders in crossflow. Journal of Fluid Mechanics. 2019; 861: 349–381. doi: 10.1017/jfm.2018.913
24. Zhang Q, Jiang B, Huang W, et al. Effect of wellhead tension on buckling load of tubular strings in vertical wells. Journal of Petroleum Science and Engineering. 2018; 164: 351–361. doi: 10.1016/j.petrol.2018.01.059
25. Govardhan R, Williamson CHK. Modes of vortex formation and frequency response of a freely vibrating cylinder. Journal of Fluid Mechanics. 2000; 420: 85–130. doi: 10.1017/S0022112000001233
26. Williamson CHK, Govardhan R. Vortex-induced vibrations. Annual Review of Fluid Mechanics. 2004; 36(1): 413–455. doi: 10.1146/annurev.fluid.36.050802.122128